
Accelerated First-Order Optimization under Nonlinear Constraints

Michael Muehlebach¹ Michael I. Jordan²

Abstract

We exploit analogies between first-order algorithms for constrained optimization and non-smooth dynamical systems to design a new class of accelerated first-order algorithms for constrained optimization. Unlike Frank-Wolfe or projected gradients, these algorithms avoid optimization over the entire feasible set at each iteration. We prove convergence to stationary points even in a nonconvex setting and we derive rates for the convex setting. An important property of these algorithms is that constraints are expressed in terms of velocities instead of positions, which naturally leads to sparse, local and convex approximations of the feasible set (even if the feasible set is nonconvex). Thus, the complexity tends to grow mildly in the number of decision variables and in the number of constraints, which makes the algorithms suitable for machine learning applications. We apply our algorithms to a compressed sensing and a sparse regression problem, showing that we can treat nonconvex ℓ^p constraints ($p < 1$) efficiently, while recovering state-of-the-art performance for $p = 1$.

1. Introduction

Optimization plays an essential role in machine learning by providing a theoretical foundation on which algorithms, systems, and datasets can be brought together at unprecedented scales. The focus in recent years has been on unconstrained optimization and first-order algorithms, as this has sufficed for many applications in pattern recognition. In particular, theoretical work on rates, lower bounds, and choice of step sizes has focused on the unconstrained setting. This is despite the important role that constraints play in applications; indeed, emerging problems in machine learning involve decision-making in the real world, which often includes

safety constraints, economic constraints, and constraints arising from the presence of multiple decision-makers. Similarly, control-theoretic problems often involve interactions with physical, biological, and social systems, whose laws are generally expressed in terms of fundamental constraints.

In practice, constraints can sometimes be treated via reparametrizations, which transform the constrained problem into an unconstrained one. Unfortunately, such a reparameterization affects the conditioning and thereby the convergence rates of algorithms, and it might be difficult to find reparameterizations that are computationally efficient. This motivates a nascent trend to focus directly on constrained optimization while retaining the advantages of first-order algorithms for machine learning.

The most prominent first-order methods that treat constraints are projected gradient algorithms and the Frank-Wolfe method. Both involve an inner loop inside of an overall procedure that optimizes over the entire feasible set. While this enables a relatively straightforward convergence analysis that parallels the unconstrained case, the procedure is only efficient if the feasible set has a simple structure, such as a norm ball, a low-dimensional hyperplane, or a probability simplex. If the feasible set fails to enable closed-form projections or closed-form Frank-Wolfe updates, algorithm designers often turn to interior point or sequential quadratic programming methods. These are significantly more complex, rely on second-order information, and their iteration complexity scales less favorably with the problem size.

Our goal in the current paper is to address the need for learning-friendly first-order methods that can handle constraints. We present a new class of first-order methods that are applicable to a wide range of problems in machine learning. An important simplification, compared to Frank-Wolfe or projected gradients, is that these methods rely exclusively on local approximations of the feasible set. While the entire feasible set might be described with a very large (or even infinite) number of *nonlinear* constraints, these local approximations, which are well-defined for feasible and infeasible points, typically consist of a small number of *linear* constraints. This substantially reduces the amount of computation required for a single iteration, and results in an expanded range of possible applications in machine learning. We highlight the efficiency of our methods by

¹Learning and Dynamical Systems, Max Planck Institute for Intelligent Systems, Tuebingen, Germany ²Electrical Engineering and Computer Science Department, University of California Berkeley, Berkeley, USA. Correspondence to: Michael Muehlebach <michaelm@tuebingen.mpg.de>.

including numerical results from a compressed sensing and a sparse regression problem, which include nonconvex ℓ^p regularization with $p < 1$. A detailed summary that connects the proposed methods with the literature can be found in App. A.

Notation and outline: We consider the following problem:

$$\min_{x \in \mathbb{R}^n} f(x), \quad \text{s.t.} \quad g(x) \geq 0, \quad (1)$$

where the function $f : \mathbb{R}^n \rightarrow \mathbb{R}$ defines the objective, the function $g : \mathbb{R}^n \rightarrow \mathbb{R}^{n_g}$ the constraints, and where n and n_g are positive integers. The set of all real numbers is denoted by \mathbb{R} and the set of all integers by \mathbb{Z} . In order to simplify our exposition, we do not explicitly include equality constraints—these can be treated in a similar way. The function f is assumed to be such that $f(x) \rightarrow \infty$ for $|x| \rightarrow \infty$, and the set of all $x \in \mathbb{R}^n$ that satisfies $g(x) \geq 0$ is denoted by C , assumed non-empty and bounded. The boundedness of C simplifies the exposition; however, if C were unbounded, the coercivity of f could be used to add the additional constraint $f(x) \leq f(x_0)$, where x_0 is a feasible initial condition, at which point C would be bounded again. The functions f and g are continuously differentiable and have a Lipschitz continuous gradient. Combined with the properties of C this guarantees that the minimum in (1) is attained. Moreover, the indicator function of a closed convex set $A \subset \mathbb{R}^n$ is denoted by ψ_A , and the subdifferential of the indicator function at $x \in A$ is denoted by $\partial\psi_A(x)$.

We note that non-smooth constraints can in many cases be reformulated (or approximated) such that the above assumptions on g are met. In case of an ℓ^p -norm constraint, this leads for example to

$$\sum_{i=1}^n |x_i|^p \leq 1 \Leftrightarrow \sum_{i=1}^n \bar{x}_i^p \leq 1, \quad -\bar{x}_i \leq x_i \leq \bar{x}_i, \quad i = 1, \dots, n, \quad (2)$$

where $\bar{x}_i \in \mathbb{R}$, $i = 1, \dots, n$ are additional decision variables.

We will mostly frame optimization problems in terms of continuous-time dynamical systems, where the equilibria of the dynamics correspond to the stationary points of (1). The continuous-time point of view often provides important (qualitative) intuition, simplifies convergence arguments, and exposes important links to dynamical and mechanical systems. Indeed, the recent line of work pursued by Su et al. (2016), Wibisono et al. (2016), França et al. (2020) and others has shown that continuous-time models provide not only a means to understand and derive upper bounds on the iteration complexity of algorithms but also lower bounds (cf. Muehlebach & Jordan, 2020).

The paper is structured in the following way: Sec. 2 summa-

rizes earlier work of Muehlebach & Jordan (2022), which covers gradient descent and sets the stage for discussing momentum-based algorithms in Sec. 3. A variety of convergence results that capture both discrete-time and continuous-time models are presented in Sec. 4. In the nonconvex regime we establish convergence to stationary points and we derive accelerated rates in the convex regime. Sec. 5 presents numerical experiments, which include nonconvex sparse regression and compressed sensing problems. The paper concludes with a short discussion in Sec. 6.

2. Constrained Gradient Flow

One of the main ideas in Muehlebach & Jordan (2022) is to express constraints in terms of velocities instead of positions, which naturally leads to local, sparse and convex approximation of the feasible set. We begin with a brief review of this work.

Let us model an optimization algorithm as a continuous-time or discrete-time dynamical system, whose equilibria correspond to the stationary points of (1). In continuous time, the configuration of the system will be denoted by $x : [0, \infty) \rightarrow \mathbb{R}^n$, which is assumed to be absolutely continuous. A fundamental observation, lying at the heart of the current research, is that the constraint $x(t) \in C$, for all $t \geq 0$, is equivalent to the constraint $\dot{x}(t)^+ \in T_C(x(t))$, for all $t \geq 0$, $x(0) \in C$, where $T_C(x(t))$ denotes the tangent cone (in the sense of Clarke) of the set C at $x(t) \in \mathbb{R}^n$, and $\dot{x}(t)^+$ denotes the forward velocity: $\dot{x}(t)^+ := \lim_{dt \downarrow 0} (x(t+dt) - x(t))/dt$. The tangent cone $T_C(x)$ is defined as the set of all vectors v such that there exist two sequences $x_k \in C$ and $t_k \geq 0$ with $x_k \rightarrow x$, $t_k \rightarrow 0$ and $(x_k - x)/t_k \rightarrow v$. Provided that a constraint qualification holds (for example Mangasarian-Fromovitz or Abadie constraint qualification), the tangent cone can be expressed as

$$T_C(x) = \{v \in \mathbb{R}^n \mid \nabla g_i(x)^T v \geq 0, \quad \forall i \in I_x\},$$

where I_x denotes the set of active inequality constraints at x ; that is, $i \in I_x$ if $g_i(x) \leq 0$.

We therefore conclude that the constraint $x(t) \in C$, which constrains the position x , is equivalent to a constraint on the forward velocity \dot{x}^+ . We note that the velocity \dot{x} is allowed to be discontinuous and may not exist for every $t \geq 0$.¹ For example, if the trajectory x reaches the boundary of the feasible set, an instantaneous jump of the velocity might be required to ensure that x remains in C .

In discrete time, however, this equivalence between position and velocity constraints no longer holds, since $T_C(x)$ is

¹We assume that \dot{x} is of locally bounded variation, which means that on any compact interval \dot{x} has countably many discontinuity points, where left and right limits exist.

only a first-order approximation of the feasible set. Thus, implementing $(x_{k+1} - x_k) = T \nabla_{T_C}(x_k)$ may lead to infeasible iterates. Muehlebach & Jordan (2022) therefore suggest to introduce the velocity constraint $\dot{x}(t)$, which is defined as

$$V(x) := \{v \in \mathbb{R}^n \mid \exists g_i(x) \text{ s.t. } v + g_i(x) \leq 0; \exists i \in I_x\} \quad (3)$$

and includes the restitution coefficient $\beta \in [0, 1]$. The following remarks motivate (3):

- i) For $x \in C$, the set $V(x)$ reduces to the tangent cone $T_C(x)$ (assuming constraint qualification).
- ii) For a fixed $x \in \mathbb{R}^n$, $V(x)$ is a convex polyhedral set involving only the active constraints. The set $V(x)$ therefore amounts to a sparse and linear approximation of the feasible set C , even if C is nonconvex.
- iii) In continuous time, the constraint $\dot{x}(t) \in V(x(t))$ for all $t \geq 0$ implies

$$g_i(x(t)) \leq \min_{g \in V(x(0))} g_i \cdot e^{-\beta t}; \quad (4)$$

for all $t \geq 0$ and all $i \in \{1, \dots, n\}$, which can be verified with Grönwall's inequality. This means that potential constraint violations decrease at rate

The continuous-time gradient flow dynamics that were studied in Muehlebach & Jordan (2022) arise from the following conditions:

$$\dot{x}(t) + r \nabla f(x(t)) = R(t); \quad R(t) \in N_{V(x(t))}(x(t)); \quad (5)$$

for all $t \geq 0$, where $N_{V(x(t))}(x(t))$ denotes the normal cone of the set $V(x(t))$ at $x(t)$. Thus, the variable $R(t)$ can be regarded as a constraint force that imposes the constraint $\dot{x}(t) \in V(x(t))$. Moreover, for each fixed $x \in \mathbb{R}^n$, we can eliminate $R(t)$ in (5) and interpret the resulting expression as a stationarity condition with respect to $\dot{x}(t)$, which means that (5) is equivalent to

$$\dot{x}(t) := \operatorname{argmin}_{v \in V(x(t))} \frac{1}{2} \|v + r \nabla f(x(t))\|^2; \quad (6)$$

As long as $V(x(t))$ is nonempty, this guarantees the uniqueness of $\dot{x}(t)$ for every $t \geq 0$. It also provides the following natural interpretation: the forward velocity $\dot{x}(t)$ is chosen to match the unconstrained gradient flow equation $\dot{x}(t) + r \nabla f(x(t)) = 0$ as close as possible, subject to the velocity constraint $\dot{x}(t) \in V(x(t))$.

Remark 2.1. Nonemptiness of $V(x)$: If C is convex, $V(x)$ is guaranteed to be nonempty for all $x \in \mathbb{R}^n$. If C is nonconvex, nonemptiness of $V(x)$ for all x in a neighborhood of C is guaranteed if the Mangasarian-Fromovitz constraint qualification holds for all $x \in C$. We note that the

in the following sense: Provided that C is semi-algebraic or conic (these cases include all the usual functions used in optimization) there exists $\delta_0 \in \mathbb{R}^m$; $\delta_0 > 0$, such that the set $C := \{x \in \mathbb{R}^n \mid g(x) \leq \delta_0\}$ satisfies the Mangasarian-Fromovitz constraint qualification for all $x \in C$ and for all $\delta \in (0; \delta_0)$; see Bolte et al. (2018).

In discrete time, it suffices to replace $\dot{x}(t)$ by $(x_{k+1} - x_k) = T$ and $x(t)$ by x_k in order to obtain the corresponding constrained gradient-descent dynamics. The condition (6) can be interpreted as a modified projected gradient scheme, where projections over the entire feasible set are replaced with optimizations over the sparse and convex approximation $V(x_k)$. The remark about the nonemptiness of $V(x_k)$ applies in the same way.

The results from Muehlebach & Jordan (2022) establish convergence of (5) (and/or (6)) both in continuous and discrete time. In continuous time, it was shown that even when f and C are nonconvex, the trajectories (5) (and/or (6)) converge to the set of stationary points. Moreover, if f is strongly convex with strong convexity constant μ and β is set to 2μ , the trajectories converge from any initial condition to the minimizer of (1) at an exponential rate:

$$\|f(x(t)) - f(x^*)\| \leq (\|f(x(0)) - f(x^*)\| + c_1) e^{-2\mu t};$$

where κ is the condition number and δ_0 is an explicit constant that captures whether the initial condition is feasible or not. Similarly, if f is strongly convex and C is convex, the trajectories in discrete time (where $\dot{x}(t)$, $x(t)$, and $R(t)$ are replaced with $(x_{k+1} - x_k) = T$, x_k , and R_k , respectively) are guaranteed to converge to the minimizer (1) for $T = 2/(L_1 + \mu)$, $\beta < \mu$, where L_1 refers to the smoothness constant of the corresponding Lagrangian. Convergence is approximately linear in this case; see Muehlebach & Jordan (2022) for the formal statement of the results.

This implies that (5) (and/or (6)) implement gradient-flow dynamics that can handle constraints and converge linearly with the typical $1 = \mu$ -rate if the objective function f is smooth and strongly convex. The set $V(x)$ can be seen as a velocity constraint and provides a natural generalization of the tangent cone. It also reduces the computational cost for each iteration, since projections on the entire feasible set are avoided. In the next section, we generalize these ideas to algorithms that have momentum. This will naturally lead to accelerated algorithms that converge linearly at a rate of roughly $1 = \mu^2$ (if f is smooth and strongly convex) or at the sublinear rate $1 = t^2$ (if f is smooth and convex), which is a significant speedup. We will also derive discrete-time convergence results even if f and C are nonconvex.

3. Accelerated Gradient Flow

We build upon the results summarized in Sec. 2 to derive momentum-based algorithms, beginning our presentation with a derivation in continuous time. The corresponding discrete-time algorithms will be stated subsequently. A natural starting point is the work of Polyak (1964), Su et al. (2016), and Muehlebach & Jordan (2019), for example, who argued that in the *unconstrained* case, accelerated optimization algorithms can be viewed as dynamical systems described by second-order differential equations. A canonical example is the following:

$$\dot{u}(t) + 2\delta u(t) + \nabla f(x(t) + \beta u(t)) = 0, \quad (7)$$

where we use the variable $u(t) = \dot{x}(t)$ to denote the velocity (or momentum), and where $\delta \geq 0$ and $\beta \geq 0$ are damping parameters.¹

In the presence of constraints, $u(t)$ is allowed to be discontinuous, which is in sharp contrast to (7). For example, if the trajectory $x(t)$ approaches the boundary of the feasible set, an instantaneous jump in $u(t)$ might be required to ensure that $x(t)$ remains feasible. Thus, compared to (5) (or equivalently (6)), where the state $x(t)$ is absolutely continuous, we are now in a position where we allow for the state $(x(t), u(t))$ (which includes the velocity u) to be discontinuous. This means that in addition to a differential equation of the type (5), which characterizes the smooth motion, we also prescribe how the discontinuities in u can arise. If we regard $(x(t), u(t))$ as the position and velocity of a mechanical system, discontinuities in u have a mechanical meaning as impacts, which are described by a corresponding impact law. The mathematical formalism, which enables discontinuities in u , is summarized next.

We still regard the state $z := (x, u)$ to be the result of an integration process:

$$z(t) = z(t_0) + \int_{t_0}^t dz, \quad \forall t \geq t_0.$$

However, instead of the usual Lebesgue density $dz = \dot{z}(t)dt$, dz now represents a differential measure (Leine & van de Wouw, 2008a), and admits both a density with respect to the Lebesgue measure (denoted by dt), as well as a density with respect to an atomic measure (denoted by $d\eta$). As is common in non-smooth mechanics, we assume that $z(t)$ is of locally bounded variation and does not contain any singular terms. This means that $z(t)$ can be decomposed in an absolutely continuous function and piecewise constant step function (Leine & van de Wouw, 2008a). At every time t , $z(t)$ has well-defined left and right limits, $z(t)^-$

¹The variables δ, β may also depend on time. For ease of presentation we focus on the case where δ and β are fixed, but also state corresponding results for time-varying parameters.

and $z(t)^+$, even though $z(t)$ might not exist or might not be of interest. We can express the differential measure dz as $dz = \dot{z}(t)dt + (z(t)^+ - z(t)^-)d\eta$, and the integration over an interval $[t_0, t]$, which contains the time instants t_{d_i} , $i = 1, 2, \dots$, where $z(t)$ is discontinuous, yields

$$z(t)^+ = z(t_0)^- + \int_{t_0}^t \dot{z}(t)dt + \sum_{i \geq 1} z(t_{d_i})^+ - z(t_{d_i})^-.$$

As a consequence of allowing the state to be discontinuous, we need to delineate both the density $\dot{z}(t)$ with respect to the Lebesgue measure dt (which describes the smooth part of the motion) as well as the density $z(t)^+ - z(t)^-$ (which describes the non-smooth motion) for fully determining the state trajectory $z(t)$. By analogy to non-smooth mechanics (see, e.g., Studer, 2009), this can be achieved with the following measure-differential inclusion:

$$du + 2\delta u dt + \nabla f(x + \beta u)dt = \sum_{i \in I_x} \nabla g_i(x) d\lambda_i, \\ \gamma_i^+ + \epsilon \gamma_i^- \in N_{\mathbb{R}_{\leq 0}}(-d\lambda_i), \quad i \in I_x, \quad (8)$$

where $\epsilon \in [0, 1)$ is a constant, γ_i is the velocity associated with the i th constraint and is defined as

$$\gamma_i(x, u) := \nabla g_i(x)^\top u + \alpha g_i(x),$$

and where we have omitted the dependence on t .² We note that the set I_x (or $I_{x(t)}$ in full notation) is time dependent. The normal cone inclusion in (8) is illustrated with Fig. 1 and will be further discussed below. The constant ϵ has the interpretation of a restitution coefficient, whereby $\epsilon = 0$ leads to inelastic collisions, and $\epsilon = 1$ yields elastic collisions. Measure-differential inclusions are common in non-smooth mechanics and the community has established various existence results for inclusions of the type (8); see, for example, Piazza et al. (2021); Leine & van de Wouw (2008b) and references therein.

We note that if x is in the interior of the feasible set, I_x is empty, and therefore (8) reduces to (7). This means that (8) generalizes (7) from the unconstrained case to the constrained case by including the constraint $\gamma_i^+ + \epsilon \gamma_i^- \in N_{\mathbb{R}_{\leq 0}}(-d\lambda_i)$, which, as we will discuss below, describes the discontinuities of u (via Newton's impact law) and imposes the velocity constraint $u(t) \in V_\alpha(x(t))$, whenever $u(t)$ exists.

It is important to note that (8) is understood in the sense of integration: For any compact time interval $[t_0, t_1]$, (8) defines the difference $u(t_1)^+ - u(t_0)^-$, which is obtained by integrating du from t_0 to t_1 ; similarly, the difference $x(t_1)^+ - x(t_0)^-$ is obtained by integrating $u(t)dt$. This means that (8) has a very natural discretization, which will

²We will frequently do so in the following.

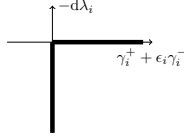


Figure 1. The figure shows the normal cone inclusion $\gamma_i^+ + \epsilon\gamma_i^- \in N_{\mathbb{R}_{\leq 0}}(-d\lambda_i)$. We note that the condition is equivalent to the complementarity condition $d\lambda_i \geq 0$, $\gamma_i^+ + \epsilon\gamma_i^- \geq 0$, $d\lambda_i(\gamma_i^+ + \epsilon\gamma_i^-) = 0$.

be discussed in the next paragraph. The last two paragraphs describe the meaning of (8). Formal convergence results in continuous and discrete time will be derived in Sec. 4.

Discretization of (8): The measure-differential inclusion (8) lends itself to the following discretization: $du = u_{k+1} - u_k$, $dt = T_k$, $d\lambda_i = \Lambda_{ki}$, $\gamma_i^+ = \gamma_i(x_k, u_{k+1})$, $\gamma_i^- = \min\{0, \gamma_i(x_k, u_k)\}$, where $T_k > 0$ is the step size.¹ This yields

$$u_{k+1} - u_k + 2\delta u_k T_k + \nabla f(x_k + \beta u_k) T_k = \sum_{i \in I_{x_k}} \nabla g_i(x_k) \Lambda_{ki},$$

$$\gamma_i(x_k, u_{k+1}) + \epsilon \min\{0, \gamma_i(x_k, u_k)\} \in N_{\mathbb{R}_{\leq 0}}(-\Lambda_{ki}),$$

$i \in I_{x_k}$. We use the newly computed momentum for updating the position x_k : $x_{k+1} = x_k + T_k u_{k+1}$, which is motivated by analogy to unconstrained optimization. (This discretization scheme is found to be superior compared to the standard Euler method; see Muehlebach & Jordan (2021).) The resulting update for u_{k+1} can be interpreted as a stationarity condition for u_{k+1} , and as a result, the proposed algorithm can be summarized as follows:

$$\tilde{u}_{k+1} = \operatorname{argmin}_{v \in \mathbb{R}^n} \frac{1}{2} |v - u_k + 2\delta u_k T_k + \nabla f(x_k + \beta u_k) T_k|^2,$$

$$\text{s.t. } \gamma_i(x_k, v) \geq -\epsilon \min\{\gamma_i(x_k, u_k), 0\}, \quad i \in I_{x_k}$$

$$x_{k+1} = x_k + T_k u_{k+1}. \quad (9)$$

Remark 2.1 applies here in the same way: If C is convex and $\epsilon = 0$, the feasible set in (9) is guaranteed to be nonempty, which means that u_{k+1} is well defined (existence and uniqueness). If C is nonconvex or $\epsilon > 0$, nonemptiness of the feasible set is guaranteed if constraint qualifications are satisfied (for example Mangasarian-Fromovitz). These constraint qualifications are generic, as discussed in Remark 2.1, which ensures that u_{k+1} is well defined as long as x_k stays in a neighborhood of the feasible set. As will be shown with our convergence analysis (see Sec. 4), we can indeed ensure that x_k remains in a neighborhood of C , the size of which we can control by choosing T_k appropriately. The pseudo-code of the full algorithm is listed in App. B.

The following remarks are important:

¹The min in γ_i^- ensures $u_{k+1} \in V_\alpha(x_k)$, which is not automatically satisfied in discrete time.

i) The update (9) has the interpretation of choosing u_{k+1} to be as close as possible to the update in the unconstrained case subject to the velocity constraint $\gamma_i(x_k, u_{k+1}) \geq -\epsilon \min\{\gamma_i(x_k, u_k), 0\}$. As a result, in case I_{x_k} is empty, (9) reduces to a standard momentum-based method; if $\beta = 0$ we obtain the heavy-ball algorithm, if $\beta \neq 0$ we obtain Nesterov's method.

ii) The update (9) includes only the constraints I_{x_k} which are active at iteration k . The constraint on v in (9) is guaranteed to be convex, even if the underlying feasible set is nonconvex. The constraints in (9) yield therefore a sparse, local and convex approximation of the feasible set. Instead of performing optimizations on the position level as is common with projected gradients or the Frank-Wolfe method, (9) suggests to constrain the velocities u_k , $k = 1, 2, \dots$

We now proceed to give an interpretation and explanation of the continuous-time dynamics (8).

Smooth motion: If $u(t)$ happens to be absolutely continuous in the interval (t_0, t_1) , its differential measure reduces to $\dot{u}(t)dt$. Similarly, the multipliers $d\lambda_i$ have only a density with respect to the Lebesgue measure dt , which we denote by $\lambda_i(t)$, i.e., $d\lambda_i = \lambda_i(t)dt$. As a result, (8) reduces to

$$\dot{u} + 2\delta u + \nabla f(x + \beta u) = \sum_{i \in I_x} \nabla g_i(x) \lambda_i, \quad (10)$$

for all $t \in (t_0, t_1)$ (a.e.). Furthermore, absolute continuity of $u(t)$ implies absolute continuity of γ_i , i.e., $\gamma_i^+ = \gamma_i^- = \gamma_i$. In the limit $dt \downarrow 0$, the inclusion in (8) therefore reduces to

$$(1 + \epsilon)\gamma_i \in N_{\mathbb{R}_{\leq 0}}(-\lambda_i) \quad \Leftrightarrow \quad \gamma_i \in N_{\mathbb{R}_{\leq 0}}(-\lambda_i),$$

for all $i \in I_{x(t)}$ and for all $t \in (t_0, t_1)$ (a.e.). ($N_{\mathbb{R}_{\leq 0}}$ is a cone; we can therefore divide by $1 + \epsilon > 0$.) The normal cone inclusion prescribing the relationship between γ_i and λ_i is similar to Fig. 1.

From a physics perspective the normal cone inclusion $\gamma_i \in N_{\mathbb{R}_{\leq 0}}(-\lambda_i)$ represents a force law, which by conic duality can also be expressed as (see again Fig. 1)

$$-\lambda_i \in N_{\mathbb{R}_{\geq 0}}(\gamma_i) = \partial\psi_{\mathbb{R}_{\geq 0}}(\gamma_i).$$

The sum $\sum_{i \in I_x} \nabla g_i(x) \lambda_i$ over $i \in I_x$ on the right-hand side of (10) therefore has a physical interpretation as a constraint force:

$$-R = -\sum_{i \in I_x} \nabla g_i(x) \lambda_i, \quad -R \in \partial\psi_{V_\alpha(x)}(u) = N_{V_\alpha(x)}(u),$$

which imposes the velocity constraint $u(t) \in V_\alpha(x(t))$ for all $t \in (t_0, t_1)$ (a.e.). By virtue of Grönwall's inequality this ensures (4).

We therefore conclude that in case of smooth motion, the measure-differential inclusion (8) generalizes the differential equation (7) from the unconstrained case to the constrained case, where the additional constraint force $R(t)$ imposes the velocity constraint $u(t) \in V_\alpha(x(t))$ (for almost all t). The introduction of the force $R(t)$ is analogous to (5).

Since the motion is smooth for almost every t , the normal cone inclusion in (8) guarantees the satisfaction of the velocity constraint $u(t) \in V_\alpha(x(t))$ (or equivalently, $\gamma_i(x(t), u(t)) \geq 0$ for all $i \in I_{x(t)}$) for all $t \geq 0$ (a.e.). However, when a new constraint arises at time t_0 , there might be a situation where $\gamma_i^-(x(t_0), u(t_0)) < 0$. In such a case an impact will be required to ensure that $\gamma_i^+(x(t_0), u(t_0)) \geq 0$. This is the subject of the next paragraph.

Non-smooth motion: In order to derive the non-smooth motion we integrate (8) over a time instant $\{t\}$, where $u(t)$ is discontinuous; that is, $u(t)^- \neq u(t)^+$. Due to the fact that the singleton $\{t\}$ has zero Lebesgue measure, we are left with the atomic parts, leading to $du = (u(t)^+ - u(t)^-)d\eta$, $d\lambda_i := \Lambda_i d\eta$,

$$u(t)^+ - u(t)^- = \sum_{i \in I_{x(t)}} \nabla g_i(x(t)) \Lambda_i, \\ \gamma_i^+ + \epsilon \gamma_i^- \in N_{\mathbb{R}_{\leq 0}}(-\Lambda_i), \quad i \in I_{x(t)}. \quad (11)$$

The normal cone inclusion should be interpreted as a generalization of Newton's impact law. For $\Lambda_i > 0$, it implies $\gamma_i^+ + \epsilon \gamma_i^- = 0$, meaning that the velocity associated to constraint i after impact, γ_i^+ , is $-\epsilon \gamma_i^-$, where γ_i^- is the velocity associated to constraint i before impact. From the discussion of the smooth motion it follows $\gamma_i(x(t_0), u(t_0))^-$ at time t_0 can only be negative if the constraint i becomes active at time t_0 ; that is, $i \notin I_{x(t)}$ for $t < t_0$ and $i \in I_{x(t)}$ for $t = t_0$. This necessitates a discontinuity in u at time t_0 , which according to the above normal cone inclusion comes in two variants: i) $\Lambda_i > 0$, which implies $\gamma_i^+ = -\epsilon \gamma_i^-$ and ii) $\Lambda_i = 0$, which implies $\gamma_i^+ \geq -\epsilon \gamma_i^-$. In variant i), the impulsive force Λ_i contributes the component $\Lambda_i \nabla g_i(x(t))$ (normal to constraint i) to the velocity jump $u(t_0)^+ - u(t_0)^-$, whereas in variant ii), there is no such contribution. Both variants ensure $\gamma_i(x(t_0), u(t_0))^+ \geq -\epsilon \gamma_i(x(t_0), u(t_0))^- \geq 0$.

The characterization of the non-smooth motion according to (11) can be interpreted as a stationarity condition for $u(t)^+$, which yields

$$u(t)^+ = \operatorname{argmin}_{v \in \mathbb{R}^n} \frac{1}{2} |v - u(t)^-|^2 \quad \text{s.t.} \\ \gamma_i(x(t), v) \geq -\epsilon \gamma_i(x(t), u(t)^-), \quad \forall i \in I_{x(t)}. \quad (12)$$

The minimization in (12) has the following interpretation: for each $u(t)^-$ there is a unique $u(t)^+$, which is chosen to

Table 1. The table summarizes convergence rates that arise from different choices of α , β , and δ . The abbreviation h. b. stands for heavy ball, N. c. p. for Nesterov constant parameters, N. v. p. for Nesterov varying parameters.

variant	α	δ	β	rate ρ
h. b.	$\sqrt{\mu}$	$\frac{\sqrt{\mu}}{3}$	0	$e^{-\sqrt{\mu}t}$
N. c. p.	$\sqrt{\mu} - \mu/2$	$\frac{\sqrt{\mu}}{1+\sqrt{\mu}}$	$\frac{1-\sqrt{\mu}}{1+\sqrt{\mu}}$	$e^{-(\sqrt{\mu}-\mu/2)t}$
N. v. p.	$\frac{2}{t+3}$	$\frac{2}{2(t+3)}$	$\frac{t}{t+3}$	$\frac{9}{(t+3)^2}$

be as close as possible to $u(t)^-$ subject to the impact law $\gamma_i^+ \geq -\epsilon \gamma_i^-$ for all $i \in I_{x(t)}$.

Equilibria of (8): The equilibria of (8) are obtained from $x(t) \equiv x_0$, $d\lambda_i \equiv \lambda_{0i} dt$, $u(t) \equiv 0$, $du \equiv 0$, where $x_0 \in \mathbb{R}^n$ and the multipliers $\lambda_{0i} \geq 0$, $i \in I_{x_0}$ are constant. As a result, (8) reduces to

$$-\nabla f(x_0) + \sum_{i \in I_{x_0}} \nabla g_i(x_0) \lambda_{0i} = 0, \\ (1 + \epsilon) \alpha g_i(x_0) \in N_{\mathbb{R}_{\leq 0}}(-\lambda_{0i}), \quad i \in I_{x_0}.$$

The normal cone inclusion can be simplified by dividing by $\alpha(1 + \epsilon) > 0$ (the normal cone is a cone), which implies that $g_i(x_0)$ and λ_{0i} satisfy the complementarity conditions

$$g_i(x_0) \geq 0, \quad \lambda_{0i} \geq 0, \quad \lambda_{0i} g_i(x_0) = 0, \quad \forall i \in I_{x_0}.$$

Hence, the equilibria of (8) satisfy the Karush-Kuhn-Tucker conditions of (1), which means that the stationary points of (1) are indeed equilibria.

4. Convergence Analysis

The following section discusses the convergence of trajectories of (8) and (9), and characterizes the rate of convergence. Without loss of generality we assume that f is normalized such that the Lipschitz constant of the gradient is unity.

Proposition 4.1. *Let $(x(t), u(t))$ be a trajectory satisfying (8) (according to Sec. 3) with $x(0) \in C$. Let f be 1-smooth, let g satisfy the Mangasarian-Fromovitz constraint qualification, and let either f be convex or $2\delta - \beta > 0$. Then, $x(t)$ converges to the set of stationary points, while $u(t)$ converges to zero. Moreover, each isolated local minimum corresponds to an asymptotically stable equilibrium in the sense of Lyapunov.*

The following proposition demonstrates that the use of momentum combined with well-chosen damping parameters indeed results in accelerated convergence rates ($\mathcal{O}(1/t^2)$ in the smooth and convex case, and $e^{-\sqrt{\mu}t}$ in the smooth and strongly convex case).¹

¹Continuous-time rates are indeed meaningful in this context,

Proposition 4.2. *Let C be convex and f be 1-smooth and either convex or strongly convex with strong convexity constant $\mu > 0$. Let the parameters α , β , δ , and ρ be chosen according to Table 1 and assume that Slater’s condition holds. Then, for any $x(0) \in \mathbb{R}^n$, $u(0) = 0$, the following holds:*

$$\begin{aligned} \min\{0, g(x(0))\}^\top \lambda^* \rho(t) &\leq f(x(t)) - f(x^*) \\ &\leq \left(\frac{\alpha^2}{2} |x(0) - x^*|^2 + f(x(0)) - f(x^*) \right) \rho(t), \end{aligned}$$

where x^* is the minimizer of (1) and λ^* is any multiplier that satisfies the Karush-Kuhn-Tucker conditions.

We also demonstrate convergence of the discrete algorithm (9) in a nonconvex and possibly stochastic setting. For simplicity we state and prove the deterministic result when $\epsilon = 0$ (as becomes apparent from the proof, the stochastic case with bounded zero-mean gradient perturbations follows from the same arguments).

Proposition 4.3. *Let $T_k = T_0/k^s$, $k = 1, 2, \dots$, for some $T_0 > 0$ and $s \in (1/2, 1)$, and let the function $\min\{0, g_1(x)\}$ have compact level sets. Let f be 1-smooth and either convex or such that $2\delta - \beta > 0$, let x_k, u_k be the iterates defined in (9) with $\epsilon = 0$ and arbitrary $(x_0, u_0) \in \mathbb{R}^{2n}$, and let g satisfy the Mangasarian-Fromovitz constraint qualification. If u_k is bounded and f has isolated stationary points, then x_k converges to a stationary point of (1), while u_k converges to zero.*

We note that the restriction $1/2 < s < 1$ can be loosened to $1/2 < s \leq 1$ if additional assumptions on the damping parameters δ and β are satisfied (this requires a slightly more detailed proof). Similarly, the assumption that f has isolated stationary points is made for simplifying the presentation. The assumption that u_k is bounded can be enforced by a simple reset strategy: if the newly computed u_{k+1} exceeds a predefined threshold, we simply set $u_{k+1} = 0$, $x_{k+1} = x_k$, and continue running the algorithm. This reset strategy reduces the total energy $|u_k|^2/2 + f(x_k)$ from step k to step $k + 1$ by a fixed amount, which implies that the function $V_k(x_k, u_k)$ (which lies at the heart of the convergence analysis) is also reduced from k to $k + 1$ for large enough k ; see App. F. Hence, the arguments used for showing convergence still apply.

We note that the behavior of algorithm (9) is complex, as it relies on a *local* approximation of the feasible set, whereby multiple constraints can become active or inactive over the

since both the Lipschitz constant of ∇f and the constant in front of ∇f in (8) are fixed to unity. This fixes the time-scale, as any reparametrization of time, i.e., $t = \tau(s)$ where $\tau : \mathbb{R}_{\geq 0} \rightarrow \mathbb{R}_{\geq 0}$ is a diffeomorphism would alter the way ∇f enters (8). We refer the reader to Muehlebach & Jordan (2020) for a more general discussion.

course of the optimization. Establishing Prop. 4.3 is therefore nontrivial (see the proof in the appendix) and requires blending different ideas from numerical analysis, optimization, and dynamical systems.

5. Numerical Examples

The following section is divided into two parts. The first part illustrates the dynamics of (8) and the discretization via (9) on a one-dimensional example and is intended to provide insights concerning the nonsmooth dynamics, as well as the discretization. The second part applies (9) to (nonconvex) compressed sensing and large-scale sparse regression problems. As we will see, our algorithm recovers state-of-the-art performance for convex relaxations, while also handling nonconvex sparsity constraints in a seamless manner (traditional projection-based methods cannot be easily extended to this setting). Further details and an additional numerical example are included in App. C.

5.1. Illustrative Example

In order to plot trajectories in the phase space we choose $f(x) = (x + 2)^2/2$ and $g(x) = (x, -x + 2)$, where x is scalar. Each constraint $g_i(x) \geq 0$ and its corresponding velocity constraint $\gamma_i(x) \geq 0$ induces a region,

$$\mathcal{R}_i := \{(x, u) \in \mathbb{R}^2 \mid g_i(x) \leq 0, \gamma_i(x, u) \leq 0\},$$

in the phase space, $i = 1, 2$, where trajectories are either non-smooth or slide along the boundary of \mathcal{R}_i . Outside of \mathcal{R}_i , the trajectories follow the smooth motion (7). Fig. 2 (left) shows the trajectories along with \mathcal{R}_1 and \mathcal{R}_2 . For a given $(x(t_0), u(t_0)^-)$ an impact happens if $g_i(x(t_0)) \leq 0$ and $\gamma_i(x(t_0), u(t_0)^-) < 0$, which ensures that $\gamma_i(x(t_0), u(t_0))^+ \geq -\epsilon \gamma_i(x(t_0), u(t_0)^-)$. In our example only the case $\gamma_i^+ = -\epsilon \gamma_i^-$ occurs, as there are no impacts where more than one constraint participates (\mathcal{R}_1 and \mathcal{R}_2 are disjoint). The coefficient of restitution ϵ therefore determines the velocity after impact. For $\epsilon = 0$ trajectories end up at the boundary of the set \mathcal{R}_i , whereas for $\epsilon > 0$ they will leave \mathcal{R}_i (in case of impact). If $g_i(x(t_0)) \leq 0$, $\gamma_i(x(t_0), u(t_0))^- = 0$, no impact happens, $(u(t_0) = u(t_0)^- = u(t_0)^+)$, and trajectories either leave \mathcal{R}_i or slide along its boundary. This depends on the contribution of the unconstrained dynamics, that is, on the vector $v_{uc}(t_0) := (u(t_0), -2\delta u(t_0) - \nabla f(x(t_0)) + \beta u(t_0))$. If $v_{uc}(t_0)$ points outwards, trajectories will leave \mathcal{R}_i and follow the unconstrained motion ($d\lambda_i = 0$). If $v_{uc}(t_0)$ points inwards, there will be a contribution from $d\lambda_i = \lambda_i(t_0)dt$, which ensures that trajectories slide along the boundary of \mathcal{R}_i .

Fig. 2 (second panel) shows the trajectories resulting from a discretization of (9) with $T_k = T = 0.1$. We can clearly see the consequences of including constraints on the velocity

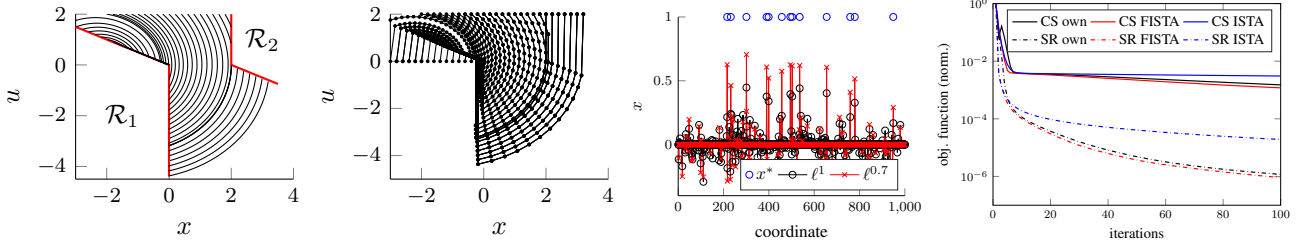


Figure 2. The first panel shows trajectories resulting from (8) (with parameters $\alpha = 0.5$, $\delta = 0.1$, $\beta = 0$, $\epsilon = 0$). The boundaries of \mathcal{R}_1 and \mathcal{R}_2 are highlighted in red. The second panel shows the results from the discretization (9) with $T_k = T = 0.1$. The third panel shows the solution vector of the compressed sensing problem with ℓ^1 and $\ell^{0.7}$ regularization. The last panel shows the objective function value (normalized) for the different methods and the two instances of (13), where CS refers to “compressed sensing” and SR to “sparse regression”.

level: Trajectories may become infeasible, since constraints enter (9) only once they are violated. Nevertheless, even for large time steps $T_k = T$ (up to $T \approx 1.8$), trajectories converge to the unique minimizer of our problem.

5.2. Compressed Sensing and Sparse Regression

We consider the following ℓ^p -regularized inverse problem:

$$\min_{x \in \mathbb{R}^n} \frac{1}{2} \|Ax - b\|_2^2 + \nu |x|_p^p, \quad (13)$$

where $|x|_p$ refers to the ℓ^p “norm” (we explicitly allow for $0 < p \leq 1$). This has numerous applications in machine learning, statistics, and signal processing (see, e.g., Hastie et al., 2009). The traditional convex approach for solving such an inverse problem is to set $p = 1$ and to leverage the fact that projections onto the ℓ^1 ball have closed-form solutions. This yields, for example, the iterative shrinkage-thresholding algorithm (ISTA) and the fast iterative shrinkage-thresholding algorithm (FISTA) (see Beck & Teboulle, 2009, Algorithm (3.1), Algorithm (4.1)-(4.3)), which are based on gradient descent and accelerated gradient descent, respectively. However, when $p < 1$, projections onto the ℓ^p “norm” ball no longer have closed-form solutions and it is unclear how to generalize ISTA/FISTA to this setting. In the following, we will highlight that this case can be handled efficiently with our approach.

We treat the regularizer as shown in (2) and apply (9). The updates can be solved in closed form; see App. C, where we also include the pseudo-code of the resulting algorithm.

In the first example, each element of $A \in \mathbb{R}^{100 \times 1000}$ is sampled from a standard normal distribution. The vector b is set to $Ax^* + n/2$, where the components of $n \in \mathbb{R}^{100}$ are sampled from a standard normal and x^* is a vector that contains zeros everywhere except for 13 randomly chosen entries that are set to one. This gives rise to a challenging and ill-conditioned optimization problem that includes 1000 decision variables. Fig. 2 (third panel) compares the results computed by our Algorithm for $p = 1$ and $p = 0.7$, whereas

the fourth panel (solid lines) compares our approach to ISTA and FISTA for $p = 1$. We note: i) the quality of the reconstruction for $p = 1$ is significantly worse compared to $p = 0.7$ (the parameter ν was tuned with five-fold cross validation in both cases) and ii) our algorithm decreases the objective function at a similar rate as FISTA for $p = 1$. All algorithms require about the same execution time per iteration.

The second example consists of an image reconstruction problem taken from Beck & Teboulle (2009), where $A = RW \in \mathbb{R}^{n \times n}$, $n = 65536$, with R representing a Gaussian blur operator, W the inverse of a three stage Haar wavelet transform, and $\nu = 2 \cdot 10^{-5}$. The problem is of considerable size and includes 65536 decision variables. Similar to the previous example, our approach is on par with the performance of FISTA for $p = 1$ (see Fig. 2, fourth panel), but is also able to solve problems with $p < 1$. Fig. 4 in App. C compares the resulting reconstruction of FISTA ($p = 1$) compared to our reconstruction $p = 0.6$, whereby the latter has much fewer artifacts. Summarizing, our approach not only achieves similar quality as FISTA for $p = 1$ (clearly outperforming ISTA) but is also able to handle nonconvex relaxations ($p < 1$). App. C contains further details about the implementation and also includes an additional numerical example.

6. Conclusion

We have introduced a new type of accelerated optimization algorithm for constrained optimization problems. By imposing constraints on velocities, rather than on positions, the algorithm avoids projections or optimizations over the entire feasible set at each iteration. This has not only the potential to reduce execution time compared to Frank-Wolfe or projected gradient schemes, but more importantly, expands the range of potential applications, as constraints are not necessarily required to be convex or to have a simple structure. We have highlighted important analogies to non-smooth dynamical systems, and characterized the algorithm’s behavior in continuous and discrete time.

Acknowledgements

We thank the German Research Foundation and the Branco Weiss Fellowship, administered by ETH Zurich, for the generous support.

References

- Beck, A. and Teboulle, M. Mirror descent and nonlinear projected subgradient methods for convex optimization. *Operations Research Letters*, 31(3):167–175, 2003.
- Beck, A. and Teboulle, M. A fast iterative shrinkage-thresholding algorithm for linear inverse problems. *SIAM Journal on Imaging Sciences*, 2(1):183–202, 2009.
- Beck, A. and Teboulle, M. Gradient-based algorithms with applications to signal-recovery problems. In *Convex Optimization in Signal Processing and Communications*, pp. 42–88. Cambridge University Press, 2011.
- Betancourt, M., Jordan, M. I., and Wilson, A. C. On symplectic optimization. *arXiv:1802.03653v2*, pp. 1–20, 2018.
- Birgin, E. G., Martínez, J. M., and Raydan, M. Inexact spectral projected gradient methods on convex sets. *IMA Journal of Numerical Analysis*, 23:539–559, 2003.
- Bloom, V., Griva, I., and Quijada, F. Fast projected gradient method for support vector machines. *Optimization and Engineering*, 17(4):651–662, 2016.
- Bolte, J., Hochart, A., and Pauwels, E. Qualification conditions in semialgebraic programming. *SIAM Journal on Optimization*, 28(2):1867–1891, 2018.
- Bubeck, S. and Cesa-Bianchi, N. Regret analysis of stochastic and nonstochastic multi-armed bandit problems. *Foundation and Trends in Machine Learning*, 5(1):1–122, 2012.
- Clarkson, K. L. Coresets, sparse greedy approximation, and the Frank-Wolfe algorithm. *ACM Transactions on Algorithms*, 6(4):1–30, 2010.
- Combettes, C. W. and Pokutta, S. Boosting Frank-Wolfe by chasing gradients. *Proceedings of Machine Learning Research*, 119:2111–2121, 2020.
- Diakonikolas, J. and Jordan, M. I. Generalized momentum-based methods: A Hamiltonian perspective. *SIAM Journal on Optimization*, 31(1):915–944, 2021.
- França, G., Sulam, J., Robinson, D. P., and Vidal, R. Conformal symplectic and relativistic optimization. *Journal of Statistical Mechanics: Theory and Experiment*, 2020(12):1–30, 2020.
- Garber, D. and Hazan, E. Faster rates for the Frank-Wolfe method over strongly-convex sets. *Proceedings of Machine Learning Research*, 37:541–549, 2015.
- Glocker, C. *Set-Valued Force Laws*. Springer, 2001.
- Gonçalves, D. S., Mucherino, A., Lavor, C., and Liberti, L. Recent advances on the interval distance geometry problem. *Journal of Global Optimization*, 69(3):525–545, 2017.
- Hastie, T., Tibshirani, R., and Friedman, J. *The Elements of Statistical Learning*. Springer, second edition, 2009.
- Hazan, E. and Kale, S. Projection-free online learning. *Proceeding of the International Conference on Machine Learning*, pp. 1–8, 2012.
- Jaggi, M. Revisiting Frank-Wolfe: Projection-free sparse convex optimization. *Proceedings of Machine Learning Research*, 28(1):427–435, 2013.
- Krichene, W., Bayen, A. M., and Bartlett, P. L. Accelerated mirror descent in continuous and discrete time. *Advances in Neural Information Processing Systems 28*, pp. 2845–2853, 2015.
- Leine, R. I. and van de Wouw, N. *Stability and Convergence of Mechanical Systems with Unilateral Constraints*. Springer, 2008a.
- Leine, R. I. and van de Wouw, N. Uniform convergence of monotone measure differential inclusions: With application to the control of mechanical systems with unilateral constraints. *International Journal of Bifurcation and Chaos*, 18(5):1435–1457, 2008b.
- Moreau, J. J. Unilateral contact and dry friction in finite freedom dynamics. In *Nonsmooth Mechanics and Applications*, pp. 1–88. Springer, 1988.
- Muehlebach, M. and Jordan, M. I. A dynamical systems perspective on Nesterov acceleration. *Proceedings of Machine Learning Research*, 97:4656–4662, 2019.
- Muehlebach, M. and Jordan, M. I. Continuous-time lower bounds for gradient-based algorithms. *Proceedings of Machine Learning Research*, 119:7088–7096, 2020.
- Muehlebach, M. and Jordan, M. I. Optimization with momentum: Dynamical, control-theoretic, and symplectic perspectives. *Journal of Machine Learning Research*, 22(73):1–50, 2021.
- Muehlebach, M. and Jordan, M. I. On constraints in first-order optimization: A view from non-smooth dynamical systems. *Journal of Machine Learning Research*, 23(256):1–47, 2022.

- Nemirovski, A. S. and Yudin, D. B. *Problem Complexity and Method Efficiency in Optimization*. John Wiley & Sons, 1983.
- Nesterov, Y. *Introductory Lectures on Convex Optimization - A Basic Course*. Springer Science+Business Media, LLC, 2004.
- Piazza, L. D., Marraffa, V., and Satco, B. Measure differential inclusions: Existence results and minimum problems. *Set-Valued and Variational Analysis*, 29(2):361–382, 2021.
- Polyak, B. T. Some methods of speeding up the convergence of iteration methods. *USSR Computational Mathematics and Mathematical Physics*, 4(5):1–17, 1964.
- Polyak, B. T. *Introduction to Optimization*. Optimization Software, Inc., 1987.
- Rockafellar, R. T. *Convex Analysis*. Princeton University Press, 1970.
- Studer, C. *Numerics of Unilateral Contacts and Friction*. Springer, 2009.
- Su, W., Boyd, S., and Candès, E. J. A differential equation for modeling Nesterov’s accelerated gradient method: Theory and insights. *Journal of Machine Learning Research*, 17(153):1–43, 2016.
- Teel, A. Asymptotic convergence from l_{∞} stability. *IEEE Transactions on Automatic Control*, 44(11):2169–2170, 1999.
- Wang, C. and Liu, Q. Convergence properties of inexact projected gradient methods. *Optimization*, 55(3):301–310, 2006.
- Wibisono, A., Wilson, A. C., and Jordan, M. I. A variational perspective on accelerated methods in optimization. *Proceedings of the National Academy of Sciences*, 113(47):E7351–E7358, 2016.
- Zhang, M., Shen, Z., Mokhtari, A., Hassani, H., and Karbasi, A. One sample stochastic Frank-Wolfe. *Proceedings of Machine Learning Research*, 108:4012–4023, 2020.

A. Related work

Our treatment builds on recent progress in using tools from continuous-time dynamical systems to analyze discrete-time algorithms in gradient-based optimization (Su et al., 2016; Wibisono et al., 2016; Diakonikolas & Jordan, 2021; Krichene et al., 2015; França et al., 2020; Betancourt et al., 2018; Muehlebach & Jordan, 2019; 2020; 2021). Much of this work aims at understanding accelerated first-order optimization methods, such as Nesterov’s algorithm, by exposing links between differential and symplectic geometry, dynamical systems, and mechanics. While in the absence of constraints these analogies result in *smooth* dynamical systems, the following article presents analogies between constrained optimization and *non-smooth* dynamical systems. Indeed, one of the closest point of contacts with existing literature is the notion of Moreau time-stepping in non-smooth mechanics (Moreau, 1988). The important feature of Moreau time-stepping, which also lies at the heart of our work, is that smooth and non-smooth motion is treated on equal footing, which is achieved by discretizing a certain kind of differential inclusion (see, e.g., Glocker, 2001; Studer, 2009).

Our approach can also be interpreted through the lens of the projected gradient methodology and indeed it has certain similarities to inexact projected gradient methods, as proposed in Wang & Liu (2006) and Birgin et al. (2003). While projected gradient approaches have been successfully applied in various machine learning problems (see, e.g., Beck & Teboulle, 2011; Bloom et al., 2016), the Frank-Wolfe algorithm has also received considerable attention in recent years (Jaggi, 2013). The appeal of Frank-Wolfe is further increased by the fact that it provides a unified framework for many first-order machine learning algorithms in constrained settings, including support vector machines, online estimation of mixtures of probability densities, and boosting (Clarkson, 2010). Recent results extend the Frank-Wolfe algorithm to the stochastic setting (Hazan & Kale, 2012; Zhang et al., 2020), or improve on its relatively slow convergence rate (Garber & Hazan, 2015; Combettes & Pokutta, 2020).

In some cases constraints can be handled very efficiently with mirror descent, (Nemirovski & Yudin, 1983, Ch. 3), where a non-Euclidean metric is introduced that adapts gradient descent to the specific type of objective function or the specific type of constraints at hand (Beck & Teboulle, 2003). Although mirror descent is based on projections onto the feasible set, the non-Euclidean metric can improve on problem-specific constants. An important machine learning example is the optimization of linear functions over the unit simplex, which has applications in online learning (Bubeck & Cesa-Bianchi, 2012).

Compared to projected gradients, mirror descent, and the Frank-Wolfe algorithm, our approach avoids optimizing over the entire feasible set at each iteration and instead relies on sparse, local and convex approximations. This article focuses on accelerated gradient descent, building on the recent results of Muehlebach & Jordan (2022), which treats gradient descent. Including constraints in momentum-based algorithms is challenging: The presence of constraints requires a need for sudden and large changes in momentum (impacts) in order to avoid infeasible iterates. This requires us to not only characterize the smooth motion (if constraints are absent or the solution slides along the boundary of the feasible set), but also the non-smooth motion (if the solution suddenly hits the boundary of the feasible set).

Specific problems, which have the potential to benefit from our approach include planning problems in reinforcement learning and/or optimal control, optimizations over nonconvex matrix manifolds (such as the set of orthogonal matrices), distance geometry problems that arise in computational chemistry/NMR spectroscopy, see for example Gonçalves et al. (2017), or supervised learning tasks that involve nonlinear constraints (for example in an imitation learning framework, where nonlinear constraints arise from stability requirements on the closed-loop system). We will also demonstrate our approach on an ℓ^p regularized inverse problems that arises in compressed sensing and signal processing, where we are not only able to obtain state-of-the-art results for $p = 1$, but can also seamlessly handle the regime $0 < p < 1$, see App. C.

B. Pseudo-code of Algorithm (9)

This section lists the pseudo-code of the resulting discrete-time algorithm (9).

Require: damping parameters $\beta \geq 0, \delta > 0$ { δ, β typically below 1; δ, β can be time varying}
Require: step size $T_k, k = 0, 1, \dots$ { $1/T_k \sim$ smoothness constant of the objective}
Require: constants $\alpha > 0, 0 \leq \epsilon \leq 1$ { α should be chosen such that $\alpha T_k \leq 1$ }
Require: initial condition $x_0 \in \mathbb{R}^n, u_0 \in \mathbb{R}^n$ {usually $u_0 = 0$ }
Require: $\epsilon_{\text{sol}} \geq 0, \epsilon_{\text{const}} \geq 0$ {solution tolerance, constraint tolerance}
Require: objective f and constraints g
 $x_k \leftarrow x_0, u_k \leftarrow u_0$

```

for  $k = 0, 1, \dots$  do
     $r_k \leftarrow u_k - 2\delta T_k u_k - \nabla f(x_k + \beta u_k) T_k$  {unconstrained update}
     $w \leftarrow \{\}$ 
     $W \leftarrow \{\}$ 
    for  $i = 1, \dots, n_g$  do
        if  $g_i(x_k) \leq \epsilon_{\text{const}}$  then
             $w \leftarrow (w, -\alpha g_i(x_k) - \epsilon \min\{\nabla g_i(x_k)^\top u_k + \alpha g_i(x_k), 0\})$  {add violated constraint}
             $W \leftarrow (W, \nabla g_i(x_k)^\top)$  {add violated constraint}
        end if
    end for
     $u_{k+1} \leftarrow \operatorname{argmin}_{v \in \mathbb{R}^n} |v - r_k|^2 \text{ s.t. } Wv \geq w$  {solve the quadratic program (9)}
     $x_k \leftarrow x_k + T_k u_{k+1}$  {update positions}
     $u_k \leftarrow u_{k+1}$  {update velocities}
    if  $|u_{k+1}| \leq \epsilon_{\text{sol}}$  then
        break
    end if
end for
    
```

C. Numerical Examples

C.1. Compressed Sensing and Sparse Regression

We consider the ℓ^p regularized inverse problem as stated in (13), which we state again for completeness

$$\min_{x \in \mathbb{R}^n} \frac{1}{2} \|Ax - b\|_2^2 + \nu |x|_p^p,$$

where $|x|_p$ refers to the ℓ^p “norm” (we explicitly allow for $0 < p \leq 1$). The setting considered in Beck & Teboulle (2009) is obtained for $p = 1$, resulting in a convex, but nonsmooth objective. In our setting, we allow for $p < 1$, which results in a nonconvex objective and show that our algorithm can easily deal with this situation, while maintaining state-of-the-art performance for $p = 1$. For $p = 1$, we compare our method to the iterative shrinkage-thresholding algorithm (ISTA) and to the fast iterative shrinkage-thresholding algorithm (FISTA) with constant step-sizes (see Beck & Teboulle, 2009, Algorithm (3.1), Algorithm (4.1)-(4.3)). Both methods are based on ℓ^1 regularization and exploit the fact that the proximal operator $\operatorname{prox}_{\nu|\cdot|_1} : \mathbb{R}^n \rightarrow \mathbb{R}^n$,

$$\operatorname{prox}_{\nu|\cdot|_1}(y) := \operatorname{argmin}_{x \in \mathbb{R}^n} \nu |x|_1 + \frac{1}{2} \|x - y\|_2^2, \quad (14)$$

has a closed-form solution for any $\nu > 0$. The important contribution of Beck & Teboulle (2009) was to propose FISTA and show that it is guaranteed to achieve a non-asymptotic $\mathcal{O}(1/k^2)$ rate despite the fact that the objective function is non-smooth. This is in sharp contrast to ISTA, which is guaranteed to converge with a non-asymptotic rate of $\mathcal{O}(1/k)$. The \mathcal{O} -notation hides the dependence on the initial condition and the dependence on smoothness constant measured by $|A^\top A|_2$.

However, when $p < 1$, the proximal operator in (14) fails to have a closed-form solution and it is unclear how to generalize ISTA and/or FISTA to this setting. In the following, we will show that this case can be efficiently handled with our approach.

When computing approximate solutions to (13) with algorithm (9), we introduce slack variables and reformulate the nonsmooth part of the objective as a constraint. As a result, we obtain

$$\min_{(x, \bar{x}) \in \mathbb{R}^{2n}} \underbrace{\frac{1}{2} \|Ax - b\|_2^2 + \nu \sum_{i=1}^n \bar{x}_i^p}_{:= f(x, \bar{x})}, \quad \text{s.t.} \quad -\bar{x} \leq x \leq \bar{x}, \quad (15)$$

where the inequalities hold component wise and also imply $\bar{x} \geq 0$. We now apply (9) to (15) and start by defining the constraint function g as $g(x, \bar{x}) := (g_1(x, \bar{x}), g_2(x, \bar{x}))$, where $g_1(x, \bar{x}) := \bar{x} - x$ and $g_2(x, \bar{x}) := \bar{x} + x$. The decision variables (x, \bar{x}) will be represented with the iterates $x_k \in \mathbb{R}^n$, $\bar{x}_k \in \mathbb{R}^n$, and the corresponding velocities will be denoted by $u_k \in \mathbb{R}^n$, $\bar{u}_k \in \mathbb{R}^n$, where k refers to the iteration number. As a result, the optimization in (9), which is used to determine

the velocities (u_{k+1}, \bar{u}_{k+1}) can be expressed as

$$(u_{k+1}, \bar{u}_{k+1}) = \underset{(v, \bar{v}) \in \mathbb{R}^{2n}}{\operatorname{argmin}} \frac{1}{2} |v - r_k|^2 + \frac{1}{2} |\bar{v} - \bar{r}_k|^2, \quad \text{s.t.} \quad (16)$$

$$\begin{aligned} \bar{v}_i - v_i + \alpha g_{1i}(x_k, \bar{x}_k) &\geq 0, \quad \forall i \in I_{1k} \setminus I_{3k}, \\ \bar{v}_j + v_j + \alpha g_{2j}(x_k, \bar{x}_k) &\geq 0, \quad \forall j \in I_{2k} \setminus I_{3k}, \\ \bar{v}_l + \alpha g_{3l}(x_k, \bar{x}_k) &\geq 0, \quad \forall l \in I_{3k}, \end{aligned}$$

where $g_3(x, \bar{x}) := \bar{x}$ and I_{ik} denotes the index set of constraints included in g_i that are active at iteration k , that is,

$$I_{1k} := \{i \in \mathbb{Z} \mid g_{1i}(x_k, \bar{x}_k) \leq 0\}, \quad I_{2k} := \{i \in \mathbb{Z} \mid g_{2i}(x_k, \bar{x}_k) \leq 0\}, \quad I_{3k} := I_{1k} \cap I_{2k}. \quad (17)$$

We have further set the constant $\epsilon = 0$ when deriving (16) in order to simplify the exposition. Moreover, the vectors $r_k \in \mathbb{R}^n$ and $\bar{r}_k \in \mathbb{R}^n$ are given by

$$\begin{aligned} r_k &:= u_k - 2\delta T_k u_k - \nabla_x f(x_k + \beta u_k, \bar{x}_k + \beta \bar{u}_k) T_k, \\ \bar{r}_k &:= \bar{u}_k - 2\delta T_k \bar{u}_k - \nabla_{\bar{x}} f(x_k + \beta u_k, \bar{x}_k + \beta \bar{u}_k) T_k, \end{aligned} \quad (18)$$

where $\delta > 0$ and $\beta \geq 0$ are damping parameters and $T_k > 0$ denotes the step size.¹ By analyzing the Karush-Kuhn-Tucker conditions of (16) we are able to find closed-form expressions for u_{k+1} and \bar{u}_{k+1} , which take the following form:

$$\begin{aligned} u_{k+1} &= \begin{cases} \frac{1}{2}(r_{k_i} + \bar{r}_{k_i} + \alpha g_{1i}), & \text{if } \bar{r}_{k_i} - r_{k_i} + \alpha g_{1i} < 0 \wedge i \in I_{1k} \setminus I_{3k}, \\ \frac{1}{2}(r_{k_i} - \bar{r}_{k_i} - \alpha g_{2i}), & \text{if } \bar{r}_{k_i} + r_{k_i} + \alpha g_{2i} < 0 \wedge i \in I_{2k} \setminus I_{3k}, \\ r_{k_i}, & \text{otherwise,} \end{cases} \\ \bar{u}_{k+1} &= \begin{cases} \frac{1}{2}(r_{k_i} + \bar{r}_{k_i} - \alpha g_{1i}), & \text{if } \bar{r}_{k_i} - r_{k_i} + \alpha g_{1i} < 0 \wedge i \in I_{1k} \setminus I_{3k}, \\ \frac{1}{2}(-r_{k_i} + \bar{r}_{k_i} - \alpha g_{2i}), & \text{if } \bar{r}_{k_i} + r_{k_i} + \alpha g_{2i} < 0 \wedge i \in I_{2k} \setminus I_{3k}, \\ -\alpha g_{3i}, & \text{if } \bar{r}_{k_i} + \alpha g_{3i} < 0 \wedge i \in I_{3k} \\ \bar{r}_{k_i}, & \text{otherwise,} \end{cases} \end{aligned} \quad (19)$$

where the wedge-symbol refers to the logical AND, and we have omitted the dependence of g_1 , g_2 , and g_3 on (x_k, \bar{x}_k) . Once, u_{k+1} and \bar{u}_{k+1} are computed, the position updates follow $x_{k+1} = x_k + T_k u_{k+1}$ and $\bar{x}_{k+1} = \bar{x}_k + T_k \bar{u}_{k+1}$. The full algorithm is listed in Alg. 1.

Compressed Sensing Problem: Each element of $A \in \mathbb{R}^{100 \times 1000}$ is sampled from a standard normal distribution. The vector b is set to $Ax^* + n/2$, where the components of $n \in \mathbb{R}^{100}$ are sampled from a standard normal distribution and x^* is a vector that contains zeros everywhere except for 13 randomly chosen entries that are set to one. This gives rise to an ill-conditioned optimization problem (the condition number is infinite) that includes 1000 decision variables. We run Alg.1 with the parameters $T_k = T = 1.2$, $\delta = 3/(2(k+3))$, $\beta = k/(k+3)$, and $\alpha = 2/(k+3)$ according to Tab. 1. We start by comparing the results from $p = 1$ with $p = 0.7$. In both cases, the parameter ν was optimized with 5-fold cross validation and the results computed with Alg.1 are shown in Fig. 2 (third panel). The benefits of regularizing with $p < 1$ are clearly visible, since the solution obtained with $p = 0.7$ has only 76 components which have a magnitude larger than 0.01, whereas the solution obtained with $p = 1$ has more than twice as many components that are larger than 0.01. Moreover, the non-zero components of x^* correspond to peaks in the solution obtained with $p = 0.7$ and as a result, thresholding at 0.3 recovers exactly the nonzero elements of x^* . This does not apply to the solution obtained with $p = 1$, despite optimizing the choice of the regularization parameter ν .

The comparison to FISTA and ISTA is summarized in Fig. 3 (left). It is visible how the cost quickly decreases in the first couple of iterations. This initial phase corresponds to finding a solution to $Ax - b$ (there are infinitely many). The second phase, where the cost decrease more gradually, is dominated by the term $\nu |x|_p^p$. As shown in Fig. 2, the performance of our algorithm for $p = 1$ is similar to FISTA, and improves upon ISTA (as remarked earlier, FISTA and ISTA are unable to handle the case where $p < 1$). The experiments are executed in MATLAB on a Windows laptop with an 11th Generation Intel

¹When evaluating the gradient of f with respect to \bar{x} we threshold \bar{x} at 10^{-6} , that is we compute $\nabla_{\bar{x}} f(x, \max\{\bar{x}, 10^{-6}\})$, which ensures that the gradient remains bounded.

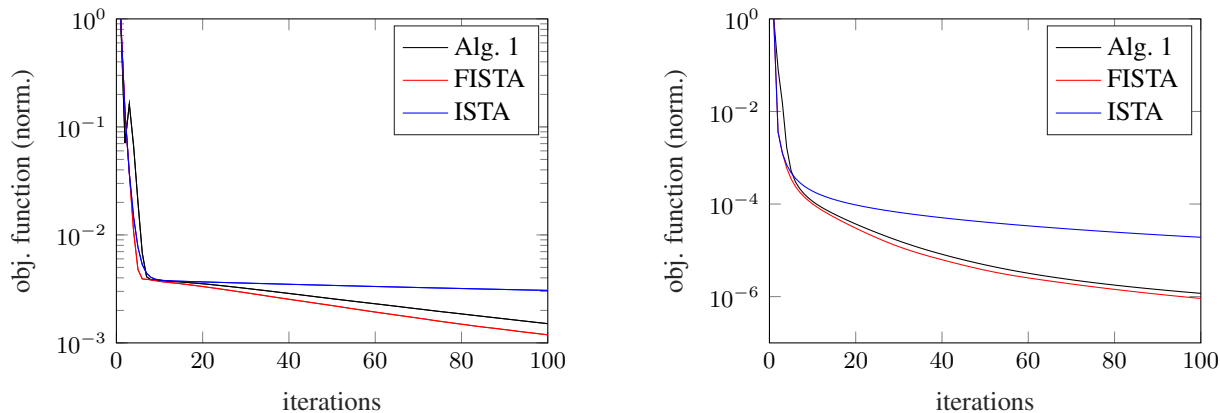


Figure 3. The figure compares the results from Alg. 1 with FISTA and ISTA. The left panel shows the results from the compressed sensing problem, while the right panel shows the results from the image reconstruction problem.

	ISTA	FISTA	Alg. 1	Alg. 1 $p = 0.7$		ISTA	FISTA	Alg. 1	Alg. 1 $p = 0.5$
100 iter.	0.01	0.02	0.02	0.04	25 iter.	1.14	1.13	1.26	1.29
250 iter.	0.02	0.02	0.05	0.08	50 iter.	1.85	1.88	2.08	2.20
500 iter.	0.04	0.04	0.08	0.16	75 iter.	2.65	2.58	2.98	3.15
750 iter.	0.05	0.07	0.12	0.24	100 iter.	3.41	3.36	3.82	4.01

Table 2. Execution time in seconds for a given number of iterations. The left panel summarizes the compressed sensing example, the right panel the image reconstruction example. We note that all algorithms have similar execution times per iteration.

Core-i7 processor and 32 gigabytes of random access memory. The execution time for ISTA, FISTA, and our implementation with $p = 1$ and $p = 0.7$ are summarized in Tab. 2 (left). We note that all algorithms have about the same execution time for a single iteration. We found that choice of the damping parameters δ and β plays a significant role. Our choice $\delta = 3/(2(k+3))$, $\beta = k/(k+3)$, and $\alpha = 2/(k+3)$, as motivated in the main article, is not optimized and a scheduling as proposed by Nesterov (2004) (Constant Step Scheme II, p.80) might improve the results.

Spare Regression Problem: We consider the task of image reconstruction, as a second example. Our setup is similar to Beck & Teboulle (2009) and we evaluate our algorithm on a 256x256 greyscale test image shown in Fig. 4 (left). As in Beck & Teboulle (2009), we applied a Gaussian blur of size nine with standard deviation four to the original image and added zero-mean Gaussian noise with standard deviation 10^{-3} , resulting in the image shown in Fig. 4 (second from left). The greyscale pixel values are represented as floating point numbers in the interval $[0, 1]$. We reconstruct the blurred and noisy image by minimizing (13), where $A = RW \in \mathbb{R}^{n \times n}$, $n = 65536$, with R representing the blur operator, W is the inverse of a three stage Haar wavelet transform, and $\nu = 2 \cdot 10^{-5}$ is the weight of the regularization. The matrix A , as well as the parameter ν are the same as in Beck & Teboulle (2009). The vector $b \in \mathbb{R}^n$ contains the pixel values of the blurred and noisy image.

We apply the following parameters when running Alg. 1: $T_k = T = 1.2$, $\delta = 3/(2(k+3))$, $\beta = k/(k+3)$, and $\alpha = 2/(k+3)$ (same as in the previous example) and compare the results to ISTA and FISTA. The execution times are listed in Table 2 and the evolution of the objective function is shown in Fig. 3 (right). We note that the optimization problem is of considerable size (65536 decision variables/131072 decision variables with 131072 constraints). We further note that although all algorithms have a comparable execution time per iteration, FISTA and Alg. 1 are able to reduce the objective function by a factor of 100 below the value of ISTA, see Fig. 3. This results in a significant difference in the quality of the output image. Fig. 4 compares the original and modified images to the result after 100 iterations of Alg. 1 ($p = 1$) and Alg. 1 ($p = 0.6$). Although both images are able to reconstruct the cameraman reasonably well, the result for $p = 0.6$ has much fewer artefacts. (The result from FISTA is the same as Alg. 1 ($p = 1$); they achieve about the same objective value, see Fig. 3.) The superiority of the result for $p = 0.6$ can most likely be attributed to the fact that the regularization with the ℓ^p “norm” with $p = 0.6$ favors a sparser solution.

Algorithm 1 Algorithm (9) applied to the image-denoising problem (13).

Require: damping parameters $\beta \geq 0, \delta > 0$; step size $T_k, L = |A|_2^2$

Require: initial condition $x_0 \in \mathbb{R}^n$

$x_k \leftarrow x_0, \bar{x}_k \leftarrow \text{abs}(x_0), u_k \leftarrow 0, \bar{u}_k \leftarrow 0$

{different initialization is also possible}

for $k = 0, 1, \dots$ **do**

$r_k \leftarrow u_k - 2\delta T_k u_k - \nabla_x f(x_k + \beta u_k, \bar{x}_k + \beta \bar{u}_k) T_k / L$

{compute unconstrained update}

$\bar{r}_k \leftarrow \bar{u}_k - 2\delta T_k \bar{u}_k - \nabla_{\bar{x}} f(x_k + \beta u_k, \bar{x}_k + \beta \bar{u}_k) T_k / L$

for $i = 0, 1, \dots, n$ **do**

$g_{1i} \leftarrow \bar{x}_{ki} - x_{ki}$

{evaluate constraints}

$g_{2i} \leftarrow \bar{x}_{ki} + x_{ki}$

$g_{3i} \leftarrow \bar{x}_{ki}$

if $g_{3i} \leq 0$ **and** $\bar{r}_{ki} + \alpha g_{3i} < 0$ **then**

$u_{k+1_i} \leftarrow r_{ki}$

$\bar{u}_{k+1_i} \leftarrow -\alpha g_{3i}$

else if $g_{1i} \leq 0$ **and** $g_{3i} > 0$ **and** $\bar{r}_{ki} - r_{ki} + \alpha g_{1i} < 0$ **then**

$u_{k+1_i} \leftarrow \frac{1}{2}(r_{ki} + \bar{r}_{ki} + \alpha g_{1i})$

$\bar{u}_{k+1_i} \leftarrow \frac{1}{2}(r_{ki} + \bar{r}_{ki} - \alpha g_{1i})$

else if $g_{2i} \leq 0$ **and** $g_{3i} > 0$ **and** $\bar{r}_{ki} + r_{ki} + \alpha g_{2i} < 0$ **then**

$u_{k+1_i} \leftarrow \frac{1}{2}(r_{ki} - \bar{r}_{ki} - \alpha g_{2i})$

$\bar{u}_{k+1_i} \leftarrow \frac{1}{2}(-r_{ki} + \bar{r}_{ki} - \alpha g_{2i})$

else

$u_{k+1_i} \leftarrow r_{ki}$

$\bar{u}_{k+1_i} \leftarrow \bar{r}_{ki}$

end if

end for

$x_k \leftarrow x_k + T_k u_{k+1}$

{update positions}

$\bar{x}_k \leftarrow \bar{x}_k + T_k \bar{u}_{k+1}$

$u_k \leftarrow u_{k+1}$

{update velocities}

$\bar{u}_k \leftarrow \bar{u}_{k+1}$

end for



Figure 4. From left to right: Original image, blurred and noisy image, output after 100 iterations with Alg. 1 ($p = 1$, similar to FISTA), output after 100 iterations with Alg. 1 ($p = 0.6$). Both the results with $p = 1$ and $p = 0.6$ lead to reasonable reconstructions, however, $p = 0.6$ has fewer artifacts.

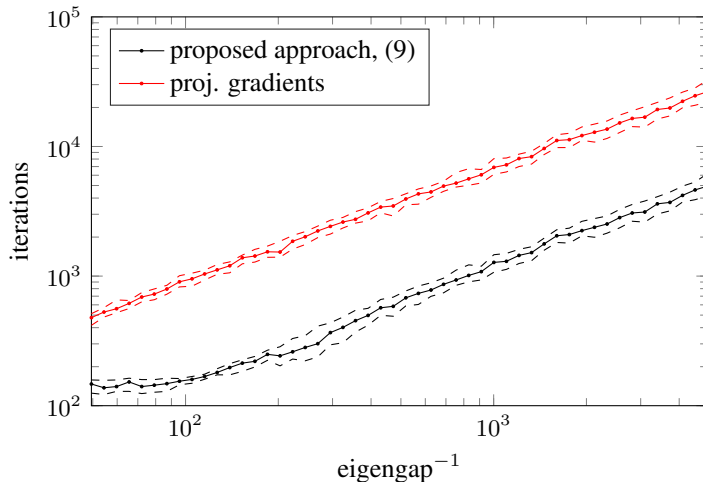


Figure 5. The figure compares the number of iterations of projected gradients and algorithm (9). We note that Frank-Wolfe cannot solve the given problem. We used the settings “Nesterov - constant parameters” in Tab. 1 (Sec. 3), with a constant stepsize $T_k = 1$ for running (9), and projected gradients was run with step size 1. Choosing a unit step size is natural, since the largest eigenvalue of H is set to 1. The dashed lines in the figure characterize the upper and lower quartile, the solid line represents the median, when randomizing over initial conditions and matrices H with a fixed “eigengap”.

C.2. Eigenvalue Problem

This section discusses an additional numerical example, which also compares the proposed algorithm (9) to Frank-Wolfe and projected gradients. More precisely, we consider the numerical solution of

$$\min_{|x| \geq 1} x^T H x,$$

where $H \in \mathbb{R}^{50 \times 50}$ is a symmetric, positive definite matrix, whose largest eigenvalue is set to unity. This is a nonconvex problem whose solution is the eigenvector belonging to the smallest eigenvalue of the matrix H . We note that Frank-Wolfe cannot be applied to this problem, since the subproblem $\min_{|s| \geq 1} s^T H x$ is unbounded below, which highlights the somewhat limited scope of Frank-Wolfe in the context of nonconvex optimization. Even when the constraint $|x| \geq 1$ is replaced by $|x| = 1$, Frank-Wolfe does not converge to a solution.

The example is motivated by the fact that the updates of both, projected gradients and (9), can be computed in closed form. The two algorithms have therefore the same computational complexity per iteration and we can compare the number of iterations. This is arguably more meaningful than comparing the runtime of different algorithms that use different procedures for solving the projection step in projected gradients and the minimization over the local approximation of the feasible set in (9). Fig. 5 shows the number of iterations as a function of the “eigengap” (the smallest spread between eigenvalues), which is the dominant factor that determines the convergence rate. We randomly generated matrices H with a fixed eigengap and sampled the components of the initial condition x_0 from a Gaussian distribution with mean zero and standard deviation ten. Fig. 5 shows the median as well as the upper and lower quartiles and highlights that our algorithm outperforms projected gradients by almost an order of magnitude.

D. Proof of Prop 4.1

From the analysis of the smooth motion in Sec. 3, we infer that $\gamma_i(x(t), u(t)) \geq 0$ for all t such that $i \in I_{x(t)}$ (a.e.). By Grönwall’s inequality, this implies $g(x(t)) \geq 0$ for all $t \geq 0$ and therefore $x(t) \in C$ for all $t \in [0, \infty)$.

We consider the following Lyapunov function

$$V(x, u) = \frac{1}{2}|u|^2 + f(x), \quad (20)$$

which is bounded below by assumption. We investigate how $V(x(t), u(t))$ evolves along the trajectories of (8). The

differential measure corresponding to $V(x(t), u(t))$ can be expressed as (Leine & van de Wouw, 2008a):

$$\begin{aligned} dV &= \frac{1}{2}(u^+ + u^-)^\top du + \nabla f(x)^\top u dt \\ &= -2\delta|u|^2 dt - (\nabla f(x + \beta u) - \nabla f(x))^\top u dt + \sum_{i \in I_x} \left(\frac{1}{2}(\gamma_i^+ + \gamma_i^-) - \alpha g_i \right) d\lambda_i. \end{aligned}$$

The second line follows from replacing du with (8), using the fact that the Lebesgue measure captures only the smooth motion, which means, for example, $(u^+)^\top u dt = (u^-)^\top u dt = |u|^2 dt$, and adding and subtracting $\alpha g_i d\lambda_i$. From the assumption $2\delta - \beta > 0$ (or alternatively by convexity of f) we can upper bound dV by

$$dV \leq -c_2|u|^2 dt + \sum_{i \in I_x} \left(\frac{1}{2}(\gamma_i^+ + \gamma_i^-) - \alpha g_i \right) d\lambda_i,$$

where $c_2 > 0$ is constant. The summand in the second part of the expression can be rewritten as

$$-\alpha g_i d\lambda_i + \frac{1}{2}(\gamma_i^+ + \epsilon \gamma_i^-) d\lambda_i + \frac{1 - \epsilon}{2}(\gamma_i^-) d\lambda_i.$$

The fact that $g_i(x(t)) = 0$ for all $i \in I_{x(t)}$ ($x(t)$ remains feasible) implies that the first term vanishes. The second term vanishes due to the complementarity condition in (8). The third term is guaranteed to be non-positive, since, on the one hand $d\lambda_i \geq 0$ (see (8)), and on the other hand, $\gamma_i^- \leq 0$ in case of impact, and $\gamma_i^- d\lambda_i = \gamma_i d\lambda_i = 0$ in case of smooth motion (see again (8)). We therefore conclude that

$$dV \leq -c_2|u|^2 dt, \quad (21)$$

which means that $V(x(t), u(t))$ is monotonically decreasing in t .

For proving convergence to stationary points, we note that since $u(t)$ is of locally bounded variation with no singular part (by assumption), it can be decomposed in an absolutely continuous function and a piecewise constant function (Lebesgue decomposition, see for example Ch. 3 of Leine & van de Wouw, 2008a). As a result, $\dot{u}(t)$ (whenever it exists) is uniformly locally integrable (see Teel, 1999). Combined with the fact that u is square integrable, which follows from (21) and the observation that V is bounded below, we conclude that $u(t) \rightarrow 0$ as $t \rightarrow \infty$ by a variant of Barbalat's lemma (see Teel, 1999). We recall that $x(t)$ is bounded (C is compact) and consider any cluster point \bar{x} of $x(t)$, which means that there exists a sequence $t_k \rightarrow \infty$ such that $x(t_k) \rightarrow \bar{x}$. We pick any $\tau > 0$ and consider

$$u(t_k + \tau)^+ - u(t_k)^- = \int_{t_k}^{t_k + \tau} du = \int_{t_k}^{t_k + \tau} -2\delta u - \nabla f(x + \beta u) dt + \sum_{i=1}^{n_g} \int_{t_k}^{t_k + \tau} \nabla g_i(x) d\lambda_i,$$

where we set $d\lambda_i = 0$ whenever $i \notin I_{x(t)}$ to simplify notation. The previous expression is guaranteed to vanish for $k \rightarrow \infty$, which by continuity of ∇g_i and ∇f means that

$$-\nabla f(\bar{x})\tau + \sum_{i=1}^{n_g} \nabla g_i(\bar{x}) \int_{t_k}^{t_k + \tau} d\lambda_i \rightarrow 0 \quad (22)$$

as $k \rightarrow \infty$. We note that by continuity of g , there exists a constant $k_0 > 0$ and $c_{1g} > 0$ such that $g_i(x(t_k)) > c_{1g}$ for all $k > k_0$ and all $i \notin I_{\bar{x}}$. From the fact that $u(t) \rightarrow 0$ we infer that for large enough k , $g_i(x(t)) > c_{1g}/2$ for all $t \in [t_k, t_k + \tau]$ and $i \notin I_{\bar{x}}$. We introduce the notation

$$\int_{t_k}^{t_k + \tau} d\lambda_i := \lambda_k^i \tau,$$

for all $k > 0$ and all $i \in \{1, 2, \dots, n_g\}$ and conclude that $\lambda_k^i \geq 0$ and, for all k large enough, $\lambda_k^i = 0$ if $i \notin I_{\bar{x}}$.

We argue next that λ_k^i is bounded for all $i \in \{1, 2, \dots, n_g\}$. We argue by contradiction and consider the sequence $(\lambda_k^1, \dots, \lambda_k^{n_g}) / |(\lambda_k^1, \dots, \lambda_k^{n_g})|$, which is guaranteed to be bounded, even though $|(\lambda_k^1, \dots, \lambda_k^{n_g})| \rightarrow \infty$. Upon dividing (22) by $|(\lambda_k^1, \dots, \lambda_k^{n_g})|$ we conclude that

$$\sum_{i=1}^{n_g} \nabla g_i(\bar{x}) \xi_i = 0,$$

where ξ denotes an accumulation point of $(\lambda_k^1, \dots, \lambda_k^{n_g})/|(\lambda_k^1, \dots, \lambda_k^{n_g})|$, which satisfies $\xi_i \geq 0$, $\xi_i = 0$ for all $i \notin I_{\bar{x}}$, and $|\xi| = 1$. However, the fact that $\xi \neq 0$ contradicts the constraint qualification, since it precludes the existence of a vector w such that $w^\top \nabla g_i(\bar{x}) > 0$ for all $i \in I_{\bar{x}}$ (which would mean $\sum_{i=1}^{n_g} w^\top \nabla g_i(\bar{x}) \xi_i > 0$). This implies that λ_k^i is bounded for all $i \in \{1, 2, \dots, n_g\}$.

We take any accumulation point of $(\lambda_k^1, \dots, \lambda_k^{n_g})$, which we denote by $\bar{\lambda}$. The accumulation point $\bar{\lambda}$ satisfies $\bar{\lambda} \geq 0$, $\bar{\lambda}_i = 0$ for all $i \notin I_{\bar{x}}$ (complementary slackness), and by (22), $-\nabla f(\bar{x}) + \sum_{i=1}^{n_g} \nabla g_i(\bar{x}) \bar{\lambda}_i = 0$. Hence, \bar{x} and $\bar{\lambda}$ satisfy the Karush-Kuhn-Tucker conditions of (1), and \bar{x} is stationary.

We conclude the section by proving asymptotic stability of isolated local minima (in the sense of Lyapunov). We therefore pick any isolated local minimum x^* and note that the function $|u|^2/2 + f(x) - f(x^*)$ is positive definite in a neighborhood of $(x^*, 0)$. We conclude from (21) that x^* is therefore stable in the sense of Lyapunov. We have already shown attractiveness (see previous paragraphs) and therefore conclude that x^* is asymptotically stable in the sense of Lyapunov.

E. Proof of Prop. 4.2

i) Heavy ball ($\alpha = \sqrt{\mu}$):

We consider the evolution of the function

$$W(x, u) = \frac{1}{2}|\alpha(x - x^*) + u|^2 + f(x) - f(x^*),$$

along the trajectories $(x(t), u(t))$. The corresponding differential measure dW is given by (Leine & van de Wouw, 2008a):

$$(\alpha(x - x^*) + (u^+ + u^-)/2)^\top (\alpha u \, dt + du) + \nabla f(x)^\top u \, dt.$$

By following the same steps as in the proof of Prop. 4.1 we obtain

$$(u^+ + u^-)/2^\top du + \nabla f(x)^\top u \, dt \leq -2\delta|u|^2 \, dt + \sum_{i \in I_x} -\alpha g_i(x) d\lambda_i.$$

However, in contrast to Prop. 4.1, we allow also for infeasible initial conditions, and therefore the term $-\alpha g_i(x) d\lambda_i$ remains. This yields the following upper bound on dW :

$$\begin{aligned} dW \leq & -(2\delta - \alpha)|u|^2 dt - \alpha(x - x^*)^\top \nabla f(x) dt + (\alpha^2 - 2\alpha\delta)(x - x^*)^\top u dt \\ & + \sum_{i \in I_x} (\alpha \nabla g_i(x)^\top (x - x^*) - \alpha g_i(x)) d\lambda_i. \end{aligned} \quad (23)$$

The fact that f is strongly convex means that the following holds

$$-(x - x^*)^\top \nabla f(x) \leq -(f(x) - f(x^*)) - \frac{\mu}{2}|x - x^*|^2.$$

In addition, convexity of C implies that each g_i is concave, and therefore

$$\nabla g_i(x)^\top (x^* - x) \geq g_i(x^*) - g_i(x) \geq -g_i(x),$$

where we used the fact that x^* is feasible for the last inequality. This concludes that the summand in (23) is non-positive since $d\lambda_i \geq 0$. Thus, after some elementary manipulations, we obtain the following upper bound on dW :

$$dW \leq -\alpha W dt - (2\delta - 3\alpha/2)|u|^2 dt \leq -\alpha W dt.$$

Applying Grönwall's inequality then implies the desired upper bound on $f(x(t)) - f(x^*)$.

The lower bound is obtained from a perturbation analysis, using an argument similar to Muehlebach & Jordan (2022). We define

$$f^*(t) := \min_{\xi \in \mathbb{R}^n} f(\xi), \quad \text{s.t.} \quad g(\xi) \geq \min\{0, g(x(0))\} e^{-\alpha t},$$

which is of the form (1), but with a modified right-hand side of the constraints. The trajectory $x(t)$ satisfies $g(x(t)) \geq \min\{0, g(x(0))\} e^{-\alpha t}$ and is therefore a feasible candidate for the above minimization, which implies $f(x(t)) \geq f^*(t)$. The

minimum is clearly attained, since f is bounded below, $f(x) \rightarrow \infty$ for $|x| \rightarrow \infty$, and the modified set of feasible points is closed. The multiplier λ^* satisfying the Karush-Kuhn-Tucker conditions of (1) captures the sensitivity of the cost function with respect to perturbations of the constraints. This means that $-\lambda^*$ is guaranteed to satisfy the following inequality (see, e.g., Rockafellar, 1970, p. 277):

$$f^*(t) - f^* \geq \min\{0, g(x(0))\}^\top \lambda^* e^{-\alpha t},$$

which combined with $f(x(t)) \geq f^*(t)$ implies the desired lower bound.

ii) Nesterov - constant parameters ($\alpha = \sqrt{\mu} - \mu/2$):

We consider again the evolution of the function

$$W(x, u) = \frac{1}{2}|a(x - x^*) + u|^2 + f(x),$$

along the trajectories $(x(t), u(t))$, where $a := \alpha$. The corresponding differential measure is given by

$$dW = (a(x - x^*) + (u^+ + u^-)/2)^\top (audt + du) + \nabla f(x)^\top udt,$$

where we have omitted the dependence on t to simplify notation (we will frequently do so in the following). From the proof of Prop. 4.1 we obtain

$$(u^+ + u^-)/2^\top du + \nabla f(x)^\top udt \leq -(2\delta + \mu\beta)|u|^2 dt + u^\top (\nabla f(x + \beta u) - \nabla f(x))dt + \sum_{i \in I_x} -\alpha g_i d\lambda_i. \quad (24)$$

Including the remaining terms yields the following upper bound on dW

$$\begin{aligned} & -(2\delta - a)|u|^2 dt + (a^2 - 2\delta a)(x - x^*)^\top udt - (\nabla f(y) - \nabla f(x))^\top udt - a(x - x^*)^\top \nabla f(y)dt \\ & \quad + \sum_{i \in I_x} (a\nabla g_i(x)^\top (x - x^*) - \alpha g_i) d\lambda_i, \end{aligned} \quad (25)$$

where we introduced the variable $y := x + \beta u$ to simplify notation. The fact that f is strongly convex means that the following holds

$$-(x - x^*)^\top \nabla f(y) \leq -(f(x) - f(x^*)) - \beta(\nabla f(x) - \nabla f(y))^\top u - \mu\beta^2|u|^2 - \mu\beta u^\top (x - x^*) - \frac{\mu}{2}|x - x^*|^2. \quad (26)$$

In addition, C is convex, which implies that each g_i is concave. As a result,

$$\nabla g_i(x)^\top (x^* - x) \geq g_i(x^*) - g_i(x) \geq -g_i(x),$$

where we used the fact that x^* is feasible for the last inequality. The summand in (25) can therefore be upper bounded by

$$(a\nabla g_i(x)^\top (x - x^*) - \alpha g_i(x)) d\lambda_i \leq (a - \alpha)g_i(x) d\lambda_i,$$

since, by definition $d\lambda_i \geq 0$. The upper bound vanishes since $a = \alpha$. Combined with (26), and after some elementary manipulations, this yields the following upper bound on dW

$$dW \leq -aWdt - (2\delta - 3a/2 + \mu\beta)|u|^2 dt - \frac{1}{2}(a\mu - a^3)|x - x^*|^2 dt + (2a^2 - 2\delta a - a\mu\beta)(x - x^*)^\top udt,$$

where we have used the fact that $1 - \beta a \geq 0$. We note that the term $2a^2 - 2\delta a - a\mu\beta$ vanishes, that $a(\mu - a^2) \geq 0$, and $2\delta - 3a/2 + \mu\beta \geq 0$ for all $\mu \in [0, 1]$. We therefore obtain $dW \leq -aWdt$, which, by Grönwall's inequality, implies the desired result.

iii) Nesterov - varying parameters ($\alpha = 2/(t + 3)$):

The proof follows the same steps. We consider the evolution of the function

$$\tilde{W}(x, u, t) = \frac{1}{2}|\tilde{a}(t)(x - x^*) + u|^2 + f(x),$$

along the trajectories $(x(t), u(t))$, where we choose $\tilde{a}(t) := \alpha(t) = 2/(t+3)$. The differential measure $d\tilde{W}$ is given by

$$d\tilde{W} = (\tilde{a}(x - x^*) + (u^+ + u^-)/2)^\top (\tilde{a}u dt + \dot{\tilde{a}}(x - x^*)dt + du) + \nabla f(x)^\top u dt,$$

where according to the chain rule the derivative of \tilde{a} with respect to t enters. This leads to two additional quadratic terms of the type

$$\tilde{a}\dot{\tilde{a}}|x - x^*|^2 dt \quad \text{and} \quad \dot{\tilde{a}}u^\top(x - x^*)dt.$$

As a result, by following the same steps as in the variant ii) (see previous section), we obtain

$$d\tilde{W} \leq -\tilde{a}\tilde{W}dt - (2\delta - 3\tilde{a}/2 + \mu\beta)|u|^2 dt - \frac{1}{2}(\tilde{a}\mu - \tilde{a}^3 - 2\tilde{a}\dot{\tilde{a}})|x - x^*|^2 dt + (2\tilde{a}^2 - 2\delta\tilde{a} - \tilde{a}\mu\beta + \dot{\tilde{a}})(x - x^*)^\top u dt.$$

We note that $2\tilde{a}^2 - 2\delta\tilde{a} + \dot{\tilde{a}}$ vanishes (in fact $\alpha = \tilde{a}$ is deliberately constructed in this way). The same applies to $2\delta - 3\tilde{a}/2$ and $\tilde{a}^3 - 2\tilde{a}\dot{\tilde{a}}$, which simplifies the above inequality to

$$d\tilde{W} \leq -\tilde{a}\tilde{W}dt - \mu\beta|u|^2 dt - \frac{1}{2}\tilde{a}\mu|x - x^*|^2 dt - \tilde{a}\mu\beta(x - x^*)^\top u dt.$$

Applying Young's inequality to the cross-term $(x - x^*)^\top u$ concludes that $d\tilde{W} \leq -\tilde{a}\tilde{W}dt$ for any $\mu \in [0, 1]$. We finally apply Grönwall's inequality, which yields

$$\tilde{W}(x(t), u(t), t) \leq \tilde{W}(x(0), u(0), 0) \exp\left(-\int_0^t \tilde{a}(s)ds\right) = \tilde{W}(x(0), u(0), 0) \frac{9}{(t+3)^2},$$

and concludes the proof.

F. Convergence Analysis of (9)

We restrict ourselves to the case $\epsilon = 0$, which allows us to restate the algorithm in the following way

$$\begin{aligned} u_{k+1} &= \underset{v \in \mathbb{R}^n}{\operatorname{argmin}} \frac{1}{2}|v - u_k + 2\delta u_k T_k + \nabla f(x_k + \beta u_k)T_k|^2 \quad \text{s.t.} \quad \gamma_i(x_k, v) \geq 0, \quad i \in I_{x_k}, \\ x_{k+1} &= x_k + T_k u_{k+1}. \end{aligned} \tag{27}$$

We note that the following arguments still apply if the gradient is stochastic, as long as the gradient-perturbations have zero mean and bounded second moments.

We start with the following three lemmas:

Lemma F.1. *Let the assumptions of Prop. 4.3 be satisfied and let $\operatorname{dist}(x, C)$ denote the distance of $x \in \mathbb{R}^n$ to the set C , that is, $\operatorname{dist}(x, C) = \min_{y \in C} |y - x|$. Then, the iterates x_k are bounded, $\operatorname{dist}(x_k, C) \rightarrow 0$, and there exists a constant $c_g > 0$ and $k_0 > 0$ such that*

$$g_i(x_k) \geq -c_g T_k,$$

for all $k \geq k_0$ and all $i \in \{1, \dots, n_g\}$.

Proof. We start by considering the first constraint, g_1 , since $\min\{g_1(x), 0\}$ has compact level sets. We distinguish the following two cases.

i) $g_1(x_k) < 0$: As a consequence of smoothness we infer that $g_1(x_{k+1}) \geq g_1(x_k) + T_k \nabla g_1(x_k)^\top u_{k+1} - T_k^2 L_{g_1} |u_{k+1}|^2/2$, where L_{g_1} is the smoothness constant of g_1 . Due to the fact that $g_1(x_k) < 0$ we have we have $1 \in I_{x_k}$ and $\nabla g_1(x_k)^\top u_{k+1} T_k \geq -\alpha T_k g_1(x_k)$. This means that

$$g_1(x_{k+1}) \geq g_1(x_k)(1 - \alpha T_k) - T_k^2 L_{g_1} c_u^2/2,$$

where we used the upper bound c_u on u_{k+1} . By the properties of the sequence $T_k = T_0/k^s$ this implies that $g_1(x_{k+1})$ is bounded below and

$$g_1(x_j) \geq -c_{g_1} T_j,$$

for some constant c_{g_1} and $j = k + 1, k + 2, \dots$, as long as $1 \in I_{x_j}$, (see for example Polyak, 1987, Chapter 2, Lemma 4 and Lemma 5).

ii) $g_1(x_k) \geq 0$ and $g_1(x_{k+1}) < 0$ (the constraint g_1 becomes active at $k + 1$). We have again $g_1(x_{k+1}) \geq \nabla g_1(x_k)^\top T_k u_{k+1} - T_k^2 L_{g_1} c_u^2 / 2$ as a result of the smoothness of g_1 and the boundedness of u_{k+1} . Due to the fact that $g_1(x_k) \geq 0$ we conclude that x_k is bounded ($\min\{g_1(x), 0\}$ has compact level sets), which means that $|\nabla g_1(x_k)| \leq \bar{c}_{g_1}$ for some constant $\bar{c}_{g_1} > 0$. Thus, we conclude

$$g_1(x_{k+1}) \geq -T_k(\bar{c}_{g_1} c_u + T_k L_{g_1} c_u^2 / 2).$$

By combining the two cases we infer that $g_1(x_k)$ is bounded below for all $k \geq 0$, which implies that x_k is bounded. We can now apply a similar reasoning to all the remaining constraints, which concludes that $\text{dist}(x_k, C) \rightarrow 0$ and $g_i(x_k) \geq -c_g T_k$ for some constant $c_g > 0$, all $i = 1, 2, \dots, n_g$, and all k large enough. \square

Lemma F.2. *Let \bar{C} be a compact set. Then, there exists a constant c_λ such that for all x with $x \in \bar{C}$ and $\lambda \in \mathbb{R}^{n_g}$ with $\lambda_i \geq 0 \forall i \in I_x$ and $\lambda_i = 0 \forall i \notin I_x$,*

$$\left| \sum_{i=1}^{n_g} \nabla g_i(x) \lambda_i \right| \geq c_\lambda |\lambda|.$$

Proof. The inequality is satisfied for $\lambda = 0$. We therefore consider the case $\lambda \neq 0$ and without loss of generality assume that $|\lambda| = 1$. We argue by contradiction and therefore assume that there are two convergent sequences λ^j and x_j with $|\lambda^j| = 1$, $\lambda_i^j \geq 0$ for all $i \in I_{x_j}$, $\lambda_i^j = 0$ for all $i \notin I_{x_j}$, and $x_j \in C$, such that $\sum_{i=1}^{n_g} \nabla g_i(x_j) \lambda_i^j \rightarrow 0$. Let the limit point of x_j be denoted by x and the limit point of λ^j by λ . As a consequence of constraint qualification, there exists a vector $w \in \mathbb{R}^n$ such that $w^\top \nabla g_i(x) \lambda_i > 0$ for all $i \in I_x$. We note that $g_i(x) > 0$ implies $g_i(x_j) > 0$ for large enough j . This concludes that $I_{x_j} \subset I_x$ and therefore

$$\sum_{i \in I_{x_j}} w^\top \nabla g_i(x) \lambda_i > c_1$$

for all large enough j and a small enough $c_1 > 0$. However, by continuity of ∇g we have

$$\sum_{i=1}^{n_g} w^\top \nabla g_i(x_j) \lambda_i^j = \sum_{i \in I_{x_j}} w^\top \nabla g_i(x) \lambda_i + \sum_{i \in I_{x_j}} w^\top \nabla g_i(x) (\lambda_i^j - \lambda_i) + \sum_{i \in I_{x_j}} w^\top (\nabla g_i(x_j) - \nabla g_i(x)) \lambda_i^j > c_1/2,$$

for all large enough j , which is a contradiction. \square

Lemma F.3. *Let the assumptions of Prop. 4.3 be satisfied. If $x_{k(j)} \rightarrow \bar{x} \in C$, $u_{k(j)} \rightarrow 0$, and $R_{k(j)}/T_{k(j)} \rightarrow \bar{R}$ for a subsequence $k(j)$, $j = 1, 2, \dots$, then \bar{x} and \bar{R} satisfy*

$$-\nabla f(\bar{x}) + \bar{R} = 0, \quad -\bar{R} \in N_{V_\alpha(\bar{x})}(0).$$

Proof. We conclude from the continuity of g_i that $g_i(\bar{x}) > 0$ implies that $g_i(x_{k(j)}) > 0$ for all j large enough and all $i \in \{1, 2, \dots, n_g\}$. This means that $I_{x_{k(j)}} \subset I_{\bar{x}}$ for all j large enough. We define a slightly modified version of $V_\alpha(x)$ as follows

$$\tilde{V}_\alpha(x) := \{u \in \mathbb{R}^n \mid \nabla g_i(x)^\top u \geq -\alpha g_i(x), \quad \forall i \in I_{\bar{x}}\},$$

which ensures that $V_\alpha(x_{k(j)}) \supset \tilde{V}_\alpha(x_{k(j)})$ for large j . Hence, the corresponding normal cones satisfy

$$N_{V_\alpha(x_{k(j)})}(u) \subset N_{\tilde{V}_\alpha(x_{k(j)})}(u),$$

for all $u \in \tilde{V}_\alpha(x_{k(j)})$, which implies, by the update rule of algorithm (9),

$$-\frac{R_{k(j)}}{T_{k(j)}} \in N_{V_\alpha(x_{k(j)})}(u_{k(j)+1}) \subset N_{\tilde{V}_\alpha(x_{k(j)})}(u_{k(j)+1}),$$

where we have used the fact that the normal cone is a cone. We now show that this implies $-\bar{R} \in N_{\tilde{V}_\alpha(\bar{x})}(0)$ and argue by contradiction. This means that there exists a $\hat{u} \in \tilde{V}_\alpha(\bar{x})$ such that $-\bar{R}^\top \hat{u} > c_1$ for a small $c_1 > 0$. From constraint

qualification, we infer that there exists a $w \in \mathbb{R}^n$ and an $\varepsilon > 0$ such that $\hat{u} + \varepsilon w \in \tilde{V}_\alpha(x_{k(j)})$ for all j sufficiently large with $-\bar{R}^\top(\hat{u} + \varepsilon w) > c_1/2$. However, this leads to a contradiction, since

$$0 \geq -\frac{R_{k(j)}^\top}{T_{k(j)}} (\hat{u} + \varepsilon w - u_{k(j)+1}) = \underbrace{-\bar{R}^\top(\hat{u} + \varepsilon w)}_{> c_1/2 > 0} + \underbrace{\bar{R}^\top u_{k(j)+1} - \left(\frac{R_{k(j)}}{T_{k(j)}} - \bar{R}\right)^\top (\hat{u} + \varepsilon w - u_{k(j)+1})}_{\rightarrow 0}.$$

This concludes that $-\bar{R} \in N_{\tilde{V}_\alpha(\bar{x})}(0)$ and the desired result follows from the fact that $\tilde{V}_\alpha(\bar{x}) = V_\alpha(\bar{x})$. \square

The following proposition will be based on diving the update (9) into the following two steps

$$\begin{aligned} \bar{x}_k &= x_k, & x_{k+1} &= \bar{x}_k + u_{k+1} T_k, \\ \bar{u}_k &= u_k - T_k f_d(x_k, u_k) + R_k, & u_{k+1} &= \bar{u}_k - T_k \nabla f(\bar{x}_k), \end{aligned} \quad (28)$$

where $f_d(x_k, u_k) := 2\delta u_k + \nabla f(x_k + \beta u_k) - \nabla f(x_k)$ contains the dissipative terms. The first step, which maps (x_k, u_k) to (\bar{x}_k, \bar{u}_k) is an update of the velocity with the dissipative terms and the constraint forces R_k , whereas the second step, which maps (\bar{x}_k, \bar{u}_k) to (x_{k+1}, u_{k+1}) is a symplectic Euler discretization that captures the conservative parts of the underlying dynamics. In the following we will exploit the fact that the second step is a symplectic map. We refer the reader to (Muehlebach & Jordan, 2021) and (Muehlebach & Jordan, 2019) for additional details.

We now prove the following lemma, which will lie at the heart of the convergence proof in discrete time.

Lemma F.4. *Let the assumptions of Prop. 4.3 be satisfied. Then, there exists a function $V_k(x, u)$, which is bounded below (uniformly in k), such that*

$$\begin{aligned} V_{k+1}(x_{k+1}, u_{k+1}) - V_k(x_k, u_k) &\leq -c_{V1} T_k |u_k|^2 - c_{V2} |R_k - T_k \nabla f(x_k)|^2 - c_{V3} T_k |R_k|^2 \\ &\quad + c_{V4} T_k^2 |u_{k+1}| + c_{V5} T_k^3 - \alpha \sum_{i \in I_{x_k}} \lambda_k^i g_i(x_k), \end{aligned}$$

for all k large enough, where $c_{V1}, c_{V2}, c_{V3}, c_{V4}, c_{V5} > 0$ are constant.

Proof. From Lemma F.1 we infer that x_k is bounded and therefore contained in a compact set, which we denote by \bar{C} . Without loss of generality we assume that f is analytic on \bar{C} (note that by the Stone-Weierstrass theorem we can find a polynomial that approximates f and ∇f arbitrarily closely, see (Muehlebach & Jordan, 2021) for details). We can now invoke Muehlebach & Jordan (Proposition 9 of 2021), which constructs the function $F_k(x, u)$ (continuous in x and u) such that

$$|\tilde{H}_k(x_{k+1}, u_{k+1}) - \tilde{H}_k(\bar{x}_k, \bar{u}_k)| \leq c_E T_k^4 \quad (29)$$

for k sufficiently large, where

$$\tilde{H}_k(x, u) := \frac{1}{2} |u|^2 + f(x) - \frac{T_k}{2} \nabla f(x)^\top u + T_k^2 F_k(x, u),$$

and c_E is constant. The function $F_k(x, u)$ is guaranteed to be bounded for $x \in \bar{C}$, $|u| \leq c_u$ (uniformly in k). We note that (29) implies that \tilde{H} is almost conserved when applying the symplectic step in (28) (in fact, the right hand side can be replaced with $(T_k)^q$ for an arbitrarily large $q > 0$). The function \tilde{H} is therefore often referred to as modified Hamiltonian and arises from the fact that the second step in (28) is a symplectic map.

We claim that the function

$$V_k(x, u) := \tilde{H}_k(x, u) + \frac{T_k d_k}{2} \nabla f(x)^\top u,$$

satisfies the desired properties, where $d_k := 1 - \bar{d} T_k > 0$ ($\bar{d} > 0$ is bounded and will be chosen subsequently). The choice $d_k = 1 - \bar{d} T_k$ is motivated by the fact that, as a result, $V_{k+1}(x, u) - V_k(x, u)$ is of order T_k^2 for $x_k \in \bar{C}$ and $|u_k| \leq c_u$. We

start by considering step 1 in (28), where we note that

$$\begin{aligned}
 \frac{1}{2}|\bar{u}_k|^2 - \frac{1}{2}|u_k|^2 &= \frac{1}{2}(\bar{u}_k - u_k)^\top(\bar{u}_k + u_k) \\
 &= -T_k f_d^\top u_k + \frac{1}{2}u_k^\top R_k + \frac{1}{2}T_k^2 |f_d|^2 - \frac{3}{4}T_k f_d^\top R_k + \frac{1}{4}|R_k|^2 \\
 &= -T_k f_d^\top u_k + \frac{1}{2}u_{k+1}^\top R_k + \frac{1}{2}T_k^2 |f_d|^2 - \frac{1}{4}T_k f_d^\top R_k - \frac{1}{4}|R_k|^2 + \frac{1}{2}T_k R_k^\top \nabla f(x_k),
 \end{aligned}$$

where we replaced u_k by u_{k+1} in the last step and omitted the arguments of $f_d(x_k, u_k)$. We further have

$$-\frac{T_k}{2}(1-d_k)\nabla f(x_k)^\top(\bar{u}_k - u_k) = -\frac{T_k}{2}(1-d_k)\nabla f(x_k)^\top(-T_k f_d + R_k),$$

which means that over step 1 in (28) the function V_k changes by

$$\begin{aligned}
 V_k(\bar{x}_k, \bar{u}_k) - V_k(x_k, u_k) &\leq -T_k f_d^\top u_k + \frac{1}{2}u_{k+1}^\top R_k + \frac{1}{2}T_k^2 |f_d|^2 - \frac{1}{4}T_k f_d^\top R_k - \frac{1}{4}|R_k|^2 \\
 &\quad + \frac{d_k}{2}T_k R_k^\top \nabla f(x_k) + \frac{T_k^2(1-d_k)}{2}\nabla f(x_k)^\top f_d \\
 &\quad + T_k^2 \nabla_u F_k(x_k, u_k)^\top(-T_k f_d + R_k) + T_k^2 c_F | -T_k f_d + R_k |^2,
 \end{aligned}$$

where $c_F > 0$ is a bound on the smoothness constant of F_k . We now proceed to the second step of (28), where we exploit the fact that \tilde{H}_k is invariant up to terms of order T_k^4 . We are therefore left with analyzing the term $T_k d_k \nabla f(x)^\top u$, which gives

$$\begin{aligned}
 V_k(x_{k+1}, u_{k+1}) - V_k(\bar{x}_k, \bar{u}_k) &\leq \frac{T_k d_k}{2}(\nabla f(x_{k+1}) - \nabla f(x_k))^\top u_{k+1} - \frac{T_k^2 d_1}{2}|\nabla f(x_k)|^2 + c_E T_k^4 \\
 &\leq \frac{T_k^2 d_k}{2}|u_{k+1}|^2 - \frac{T_k^2 d_k}{2}|\nabla f(x_k)|^2 + c_E T_k^4,
 \end{aligned}$$

where we used the fact that ∇f is 1-smooth in the second step. We therefore obtain

$$\begin{aligned}
 V_k(x_{k+1}, u_{k+1}) - V_k(x_k, u_k) &\leq -T_k f_d^\top u_k + \frac{1}{2}u_{k+1}^\top R_k - \frac{1}{4}T_k f_d^\top R_k + \frac{1}{2}T_k^2 |f_d|^2 + \frac{T_k^2 d_k}{2}|u_{k+1}|^2 \\
 &\quad - \frac{T_k \bar{d}}{4}|R_k|^2 - \frac{d_k}{4}|R_k - T_k \nabla f(x_k)|^2 - \frac{d_k}{4}T_k^2 |\nabla f(x_k)|^2 + c_{E4} T_k^4 \\
 &\quad + T_k^2 \nabla_u F_k(x_k, u_k)^\top(-T_k f_d + R_k) + T_k^2 c_F | -T_k f_d + R_k |^2.
 \end{aligned}$$

In addition we can bound $f_d^\top u_k$ and $|f_d|^2$ as follows

$$-f_d^\top u_k \leq -\bar{\delta}|u_k|^2, \quad |f_d|^2 \leq (2\delta + \beta)^2|u_k|^2,$$

where $\bar{\delta} = 2\delta$ in the convex case and $\bar{\delta} = 2\delta - \beta$ in the nonconvex case. We can thus apply Young's inequality to the term $f_d^\top R_k$, which yields

$$-\frac{1}{4}T_k f_d^\top R_k \leq \frac{1}{2}T_k \bar{\delta}|u_k|^2 + T_k \frac{|2\delta + \beta|^2}{32\bar{\delta}}|R_k|^2.$$

We further note that $|\nabla_u F_k(x_k, u_k)| \leq c_{F2}(|u_k| + |\nabla f(x_k)|)$ and apply Young's inequality to all cross-terms. This leads to

$$\begin{aligned}
 V_k(x_{k+1}, u_{k+1}) - V_k(x_k, u_k) &\leq -\frac{1}{2}T_k \bar{\delta}|u_k|^2 - \frac{T_k \bar{d}}{8}|R_k|^2 - \frac{d_k}{4}|R_k - T_k \nabla f(x_k)|^2 \\
 &\quad + \frac{T_k^2 d_k}{2}|u_{k+1}|^2 + \frac{1}{2}u_{k+1}^\top R_k + c_E T_k^4,
 \end{aligned}$$

for large enough k and for a constant \bar{d} large enough. In addition, the change of $V_{k+1}(x_{k+1}, u_{k+1}) - V_k(x_{k+1}, u_{k+1})$ can be shown to be of the order $\mathcal{O}(T_k^2|u_{k+1}| + T_k^3)$. We further infer from the update equation for u_{k+1} that $u_{k+1}^\top R_k = -\alpha \sum_{i \in I_{x_k}} \lambda_k^i g_i(x_k)$, which yields the desired result. \square

Proposition F.5. *Let the assumptions of Prop. 4.3 be satisfied. Then x_k converges to the set of stationary points of (1) and u_k converges to zero.*

Proof. From Lemma F.4 we infer the existence of a function $V_k(x, u)$ (bounded below, uniformly in k) such that

$$V_{k+1}(x_{k+1}, u_{k+1}) - V_k(x_k, u_k) \leq -c_{V1}T_k|u_k|^2 - c_{V2}|R_k|^2 + c_{V3}T_k^2 - \alpha \sum_{i \in I_{x_k}} \lambda_k^i g_i(x_k)$$

for $k \geq k_0$ and for some constants $k_0 > 0$, $c_{V1}, c_{V2}, c_{V3} > 0$, where we have used the fact that x_k and u_k are bounded. (We have abused notation by reusing c_{V1}, c_{V2}, c_{V3} .) We now invoke Lemma F.1 and Lemma F.2 for bounding the terms $\lambda_k^i g_i(x_k)$

$$\left| -\alpha \sum_{i \in I_{x_k}} \lambda_k^i g_i(x_k) \right| \leq \frac{\alpha}{c_\lambda} c_g T_k |R_k| n_g \leq \frac{c_{V2}}{2} |R_k|^2 + \frac{1}{2c_{V2}} (n_g c_g \frac{\alpha}{c_\lambda})^2 T_k^2, \quad (30)$$

where we have used Young's inequality in the second step. We therefore obtain

$$V_{k+1}(x_{k+1}, u_{k+1}) - V_k(x_k, u_k) \leq -c_{V1}T_k|u_k|^2 - \frac{c_{V2}}{2}|R_k|^2 + \bar{c}_{V3}T_k^2, \quad (31)$$

for large enough k and a modified constant $\bar{c}_{V3} > 0$. We further introduce the constants

$$-c_{V0} = \inf_k V_k(x_k, u_k), \quad c_{T1} = \sum_{k=k_0}^{\infty} T_k^2,$$

and make the following claim: There exists a subsequence $k(j), j = 1, 2, \dots$, such that

$$-c_{V1}T_{k(j)}|u_{k(j)}|^2 - \frac{c_{V2}}{2}|R_{k(j)}|^2 \geq \underbrace{\left(-\bar{c}_{V3} - \frac{V_{k_0}(x_{k_0}, u_{k_0}) + c_{V0}}{c_{T1}} - \frac{1}{c_{T1}} \right)}_{:= -c_{V4}} T_{k(j)}^2,$$

where $c_{V4} > 0$. For the sake of contradiction we assume that the claim is not true, which means that

$$-c_{V1}T_k|u_k|^2 - \frac{c_{V2}}{2}|R_k|^2 \leq -c_{V4}T_k^2$$

for all $k > 0$. However, we have chosen the constant c_{V4} deliberately in such a way that we can generate a contradiction when summing over $V_{k+1}(x_{k+1}, u_{k+1}) - V_k(x_k, u_k)$. More precisely,

$$\begin{aligned} -c_{V0} - V_{k_0}(x_{k_0}, u_{k_0}) &\leq V_N(x_N, u_N) - V_{k_0}(x_{k_0}, u_{k_0}) \leq \sum_{k=k_0}^N (-c_{V4} + \bar{c}_{V3})T_k^2 \\ &\leq \frac{-c_{V0} - V_{k_0}(x_{k_0}, u_{k_0}) - 1}{c_{T1}} \sum_{k=k_0}^N T_k^2. \end{aligned}$$

which leads to the desired contradiction since the right-hand side approaches $-c_{V0} - V_{k_0}(x_{k_0}, u_{k_0}) - 1$ for $N \rightarrow \infty$.

Upon passing to another subsequence we infer that $u_{k(j)} \rightarrow 0$, $R_{k(j)}/T_{k(j)} \rightarrow \bar{R}$, and $x_{k(j)} \rightarrow \bar{x} \in C$. By invoking Lemma F.3 we conclude that \bar{x} is stationary and \bar{x} and \bar{R} satisfy the Karush-Kuhn-Tucker conditions.

We now prove that the entire sequence converges. We infer from (31) that for any $\varepsilon > 0$ we can find an $m > 0$ such that $V_N(x_N, u_N) \leq V_m(x_m, u_m) + \varepsilon$ for all $N > m$. More precisely,

$$\sum_{k=m}^{N-1} V_{k+1}(x_{k+1}, u_{k+1}) - V_k(x_k, u_k) \leq \bar{c}_{V3}T_m^q \sum_{k=m}^{N-1} \left(\frac{T_k}{T_m} \right)^q T_k^{2-q} \leq \bar{c}_{V3}T_m^q \sum_{k=m}^{\infty} T_k^{2-q}, \quad (32)$$

where the right-hand side is of the order T_m^q , since T_k^{2-q} is summable for a small enough $q > 0$. This implies that all accumulation points of x_k, u_k must be contained in the same level set of the function $|u|^2/2 + f(x) = \lim_{k \rightarrow \infty} V_k(x, u)$. Thus, the sequence $V_k(x_k, u_k)$ converges and satisfies

$$\lim_{k \rightarrow \infty} V_k(x_k, u_k) = \lim_{k \rightarrow \infty} \left(\frac{1}{2}|u_k|^2 + f(x_k) \right) = f(\bar{x}),$$

where \bar{x} is the limit of $x_{k(j)}$ (see above). We further introduce the collection of all accumulation points of x_k, u_k , that is,

$$\omega := \bigcap_{m \geq 0} \text{cl}\{(x_k, u_k) : k > m\},$$

where cl denotes closure. We note that $\omega \subset C \times \mathbb{R}^n$ is connected (since $|x_{k+1} - x_k| \rightarrow 0$ and $|u_{k+1} - u_k| \rightarrow 0$) and for any $(x, u) \in \omega$, $|u|^2/2 + f(x) = f(\bar{x})$.

We claim that $\omega = \{(\bar{x}, 0)\}$. For the sake of contradiction, we assume the existence of a sequence $(\tilde{x}_k, \tilde{u}_k) \rightarrow (\bar{x}, 0)$, $(\tilde{x}_k, \tilde{u}_k) \in \omega$ with $(\tilde{x}_k, \tilde{u}_k) \neq (\bar{x}, 0)$ (ω is connected). We consider first the case where \bar{x} lies in the interior of C (constraints are not active). In that case \tilde{x}_k lies likewise in the interior of C for large k . However, in the absence of constraints the dynamics in (9) are smooth, which means that \tilde{x}_k and \tilde{u}_k are guaranteed to be equilibria and therefore satisfy $\tilde{u}_k = 0$ and $\nabla f(\tilde{x}_k) = 0$. However, this contradicts the fact that f has isolated stationary points. Next, we consider the case where \bar{x} lies on the boundary of C , where we infer from $(\tilde{x}_k, \tilde{u}_k) \in \omega$ that $f(\tilde{x}_k) = f(\bar{x}) - |\tilde{u}_k|^2/2$. Therefore $f(\tilde{x}_k) \leq f(\bar{x})$, $\tilde{x}_k \in C$ for all $k > 0$, which also contradicts the fact that \bar{x} is an isolated stationary point.

Thus, we conclude $\omega = \{(\bar{x}, 0)\}$ and the result follows. □